



UNIVERSITY OF
CAMBRIDGE

Department of Engineering

Knee Stabilisation Surgery: Minimising Surgical Risk in High Tibial Osteotomy

Author Name: Radhika Gupta

Supervisor: Prof. Michael Sutcliffe

Date: 1st June 2022

I hereby declare that, except where specifically indicated, the work submitted herin is my own original work.

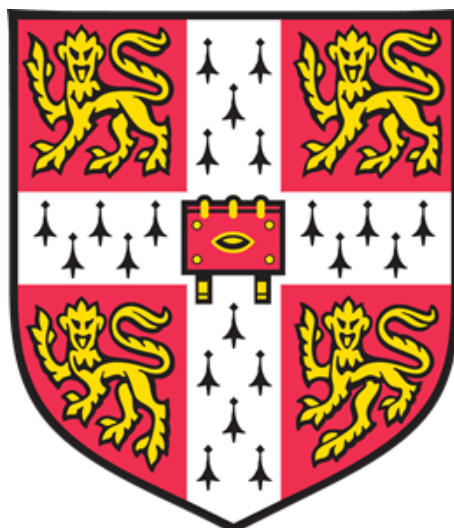
Signed _____  date _____ 01/06/2022 _____

Knee Stabilisation Surgery

Preventing Lateral Hinge Fracture in High Tibial Osteotomy

Radhika Gupta
Pembroke College

In partial fulfilment of the requirements for the
Master of Engineering



Mechanical Engineering Division
University of Cambridge
1st June 2022

Technical Abstract

Arthritis of the knee affects one in five adults aged over 45 in England [1], and is the primary reason for knee replacement surgeries. Medial opening wedge high tibial osteotomy (MOWHTO) surgery provides an alternative treatment by preserving the knee joints, rather than replacing them. It is the recommended surgery for patients aged under 60, as it offers a longer-lasting solution and greater post-operative mobility. The surgery realigns the weight-bearing axis of the leg to relieve diseased tissue of excess pressure, reducing joint pain and stiffness. However, it is not risk-free, and this project aims to minimise its risks.

During surgery, a slanted cut is made through the tibia, leaving a stretch of bone, called the *lateral hinge*, intact. The cut is opened up into a wedge to achieve the desired alignment. A fixation plate is then screwed across the gap to support the knee as it heals. The bone grows to fill the gap over the course of a few weeks, after which the plate is removed. A labelled X-ray image taken before and after MOWHTO surgery is shown in figure 1.

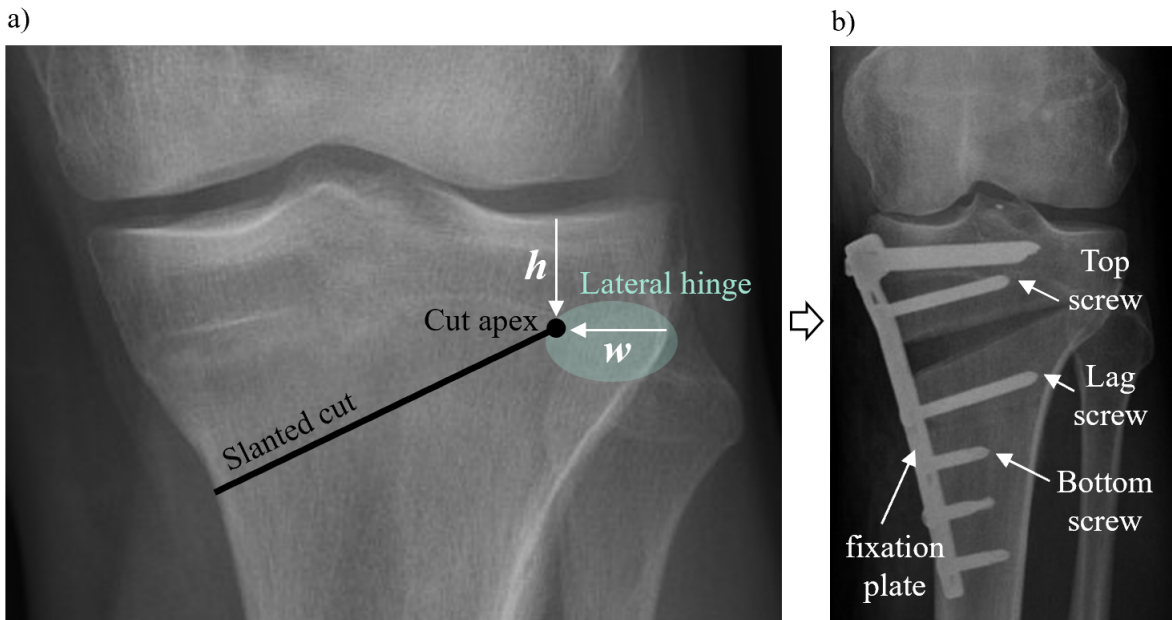


Figure 1: Labelled surgical CT scan, based on [2, 3]. a) Before MOWHTO surgery. b) After MOWHTO surgery.

Fracture of the lateral hinge is one of the most common complications associated with MOWHTO. It reduces the stability of the assembly, resulting in a loss of angular correction. Fractures may occur during the cut opening process or from loads incurred during weight-bearing. They nucleate at the cut apex (end-point). Fractures are commonly classified into three types [4]. Type I fractures propagate horizontally towards the side of the tibia and are mild. Type II fractures propagate downwards and type III up towards the top surface; both these types are more severe than type I, and have problematic clinical implications.

The first project aim was to find an optimal lateral hinge position which minimises the expected surgical risk in MOWHTO surgery. The width of the lateral hinge w and vertical distance h from the tibial plateau significantly influence the likelihood and severity of fracture, but surgical guidelines for these parameters vary across studies. A risk-minimising hinge location was desired, considering both fracture during intra-operative cut opening and post-operative stability. This work used finite element (FE) modelling of intra-operative and post-operative loading to identify

the relationship between hinge position and expected surgical risk.

Intra-operative FE results showed that stresses near the apex increase with wider hinges, and hinges closer to the tibial plateau, indicating greater fracture likelihood. These positions are also more indicative of severe type III than mild type I fracture using strain-based failure criteria. We omitted type II fractures from the analysis as they are only observed for very low hinge positions which lie beyond the recommended range. Our results agree with existing literature, and extend it by predicting the (w, h) contour across which the fracture type transitions from type I to type III. We proposed an inequality along this contour, describing where to aim the cut apex to avoid severe type III fracture: $h > 0.56w + 6.0$, with all quantities in mm.

Post-operative FE results showed that width of the lateral hinge has the greatest effect on post-operative stability; wider hinges provide better stability. Widths between 13 - 22 mm keep micromotion in the acceptable range of 100 - 200 μm , recommended by Kang et al. [5]. The post-operative analysis recommended larger hinge widths than expected, due to the anterior placement of the fixation plate in this study, in contrast to the more medial placement in other studies [6].

Results were combined from intra and post-operative FE simulations, with two additional bonds from recommendations across literature: $w < 15$ mm and $h < 20$ mm, to propose an updated ‘safe’ region for the optimal cut apex location. Within this updated region, we proposed a recommended apex position expected to minimise the surgical risk posed by MOWHTO: $w = 13$ mm, $h = 17$ mm. This position was estimated by locating the centroid of the bounded locus and imposing a bias towards a narrower hinge width due to the leniency of the post-operative $w > 13$ mm bound.

The second aim of this project was to find the relative strains at the lateral hinge during plate fixation, and to investigate the effects of changing the screw insertion order and the non-locking lag screw angle. In the case of a lateral hinge fracture, the plate fixation process ought to induce as little strain as possible at the lateral hinge to prevent further crack propagation and displacement of the fractured regions. Prior to this work, the strains at the lateral hinge during plate fixation were not well understood, nor how changes to the procedure may affect them.

We devised a simplified experiment model which mimicked the mechanical interactions between the bone, fixation plate, and screws. Screws were inserted to fix the plate to the tibia with varying insertion order, and strain was measured midway along the lateral hinge with a strain gauge. We carried out FE simulations to compare with experimental findings on varying screwing order, and to investigate the effect of changing the lag screw angle.

Experiments showed that when inserting screws in the default insertion order (top to bottom), the lag screw imposes significant tensile strains. Inserting the screws in reverse order negates undesirable tensile strains and retains the compression from the top screw, offering an improvement from the default method in the case of a type I fracture. Partly inserting the top screw before tightening the lag screw minimises strain magnitudes across all screws and may be better than the default method for avoiding fracture.

Finite element analysis (FEA) on screw order matched experimental strains when tightening the lag screw, but deviated from experimental strains when tightening the top screw. We concluded that the FE setups used to model top screw tightening need revision. Results from the lag screw angle investigation corroborated the lag angle hypothesis; angling the screw 10° or 20° distally compared to 0° reduces the tensile strains near the apex by up to 50%.

In summary, the main contributions of this work to research in knee stabilisation surgery are the proposal of an optimal cut apex position and an alternative plate fixation method to minimise surgical risk in MOWHTO surgery.

Contents

1	Introduction	4
2	Literature Review	6
2.1	Surgery details	6
2.2	Tibia Bone Material and Mechanics	7
2.3	Fracture in High Tibial Osteotomy	9
2.3.1	Fracture Mechanics	9
2.3.2	Complications and Causes of Fracture	10
2.3.3	Fracture Classification	11
2.3.4	Effect of Lateral Hinge Location	12
2.4	Plate Fixation Procedure	13
3	Project Aims and Structure	14
3.1	Optimal Osteotomy Apex Location	14
3.2	Optimal Plate Fixation Procedure	15
3.3	Project Structure	15
4	Finding the Optimal Osteotomy Apex Location	16
4.1	Problem Definition	16
4.2	Tibia model used in intra and post-operative analyses	18
4.3	Intra-operative Analysis	19
4.3.1	Methods	19
4.3.2	Fracture Type Classification	21
4.3.3	Results and Discussion	22
4.4	Post-operative Analysis	25
4.4.1	Methods	25
4.4.2	Results and Discussion	26
4.5	Surgical Implications	27
5	Investigating Plate Fixation Procedure	29
5.1	Varying Screw Insertion Order	30
5.1.1	Overview	30
5.1.2	Experimental Methods	30
5.1.3	Experimental Results and Discussion	33
5.1.4	FE Methods	35
5.1.5	FE Results and Discussion	37
5.2	Varying Lag Screw Angle	39
5.2.1	Methods	39
5.2.2	Results and Discussion	39
6	Limitations and Further Research	40
7	Conclusions	41
8	Acknowledgements	42

1 Introduction

Current surgical procedures in knee stabilisation surgery may not be as effective as they could be in preventing fracture. The focus of this study is Medial Opening Wedge High Tibial Osteotomy (MOWHTO), a knee surgery which corrects for ‘bow-leggedness’, known as the *varus deformity*. Varus involves a misalignment of the leg’s mechanical (weight-bearing) axis and both contributes to and is accelerated by knee arthritis, the most common form of arthritis in the UK [7].

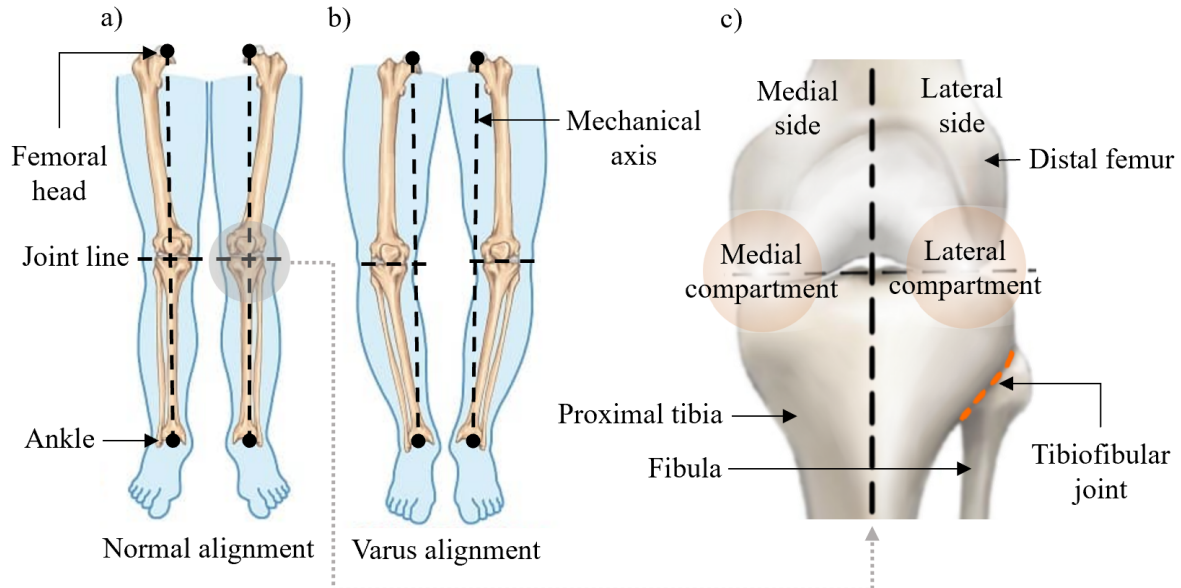


Figure 2: Diagram of human knee anatomy, based on [8, 9] a) Legs with an ideal mechanical axis. b) Legs with the varus deformity. c) The knee joint.

The ideal mechanical axis passes from the femoral head to the ankle joint, through the centre of the tibia-femur joint line [10], shown in figure 2(a) and (c). In legs affected by the varus deformity 2(b), the mechanical axis is shifted towards the medial side of the joint line, causing degeneration of cartilage at the medial compartment, pain, and joint stiffness.

MOWHTO surgery provides an alternative treatment to total knee replacement, by realigning the mechanical axis to pass through the healthy lateral compartment and thus offloading the diseased medial compartment [7, 11]. It consists of three main steps, depicted in figure 3. Before the operation, the medial side of the joint carries most of the patient’s weight, indicated by the long red arrow in figure 3a. The surgery begins with an *osteotomy*, a slanted cut through the proximal tibia. The cut leaves a stretch of bone, referred to as the *lateral hinge*, intact. Next, the cut is opened up with a bone spreader, creating a wedge shaped gap, which straightens the tibia with respect to the femur. This shifts the mechanical axis back towards the centre of the joint line for a more uniform weight distribution, indicated by the balanced green arrows in figure 3c. Finally, a fixation plate is screwed in across the opened cut to hold the bone in place as the cut heals.

The surgery provides greater post-operative mobility [12] and has a longer lifetime than knee replacement surgery, and is thus the recommended surgery for active patients less than 60 years of age [7]. It has the potential to delay the need for total knee replacement by more than 15 years in most patients [11]. However, the surgery is not risk-free. One of the most common and severe complications is the possibility of bone fracture at the lateral hinge [10, 6]. This may occur during cut opening, plate fixation, or weight-bearing after surgery. Fractures can reduce

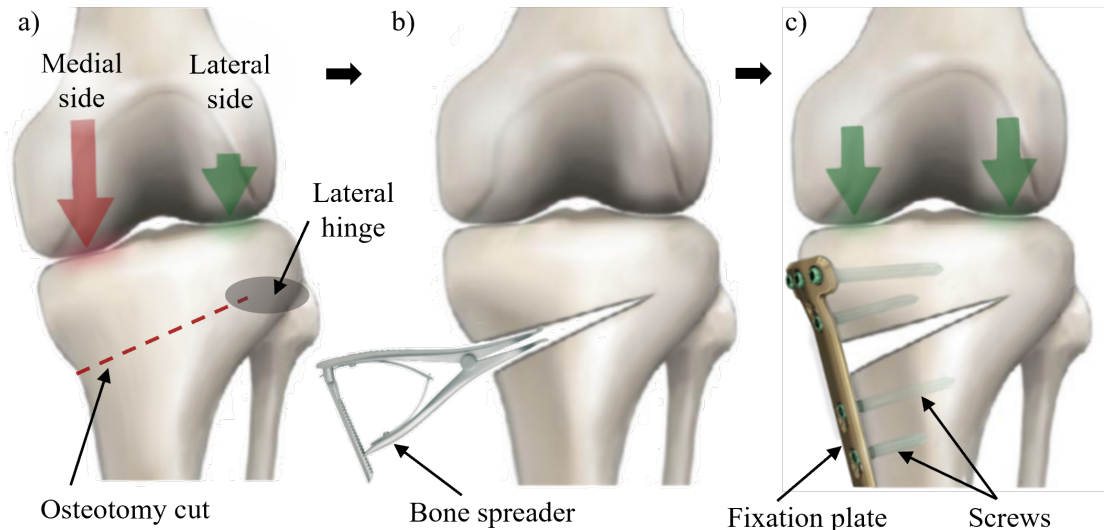


Figure 3: Medical Opening Wedge High Tibial Osteotomy (MOWHTO) surgical sequence. a) The osteotomy cut is made. Initially, the medial compartment carries most of the patient's weight, indicated by the long red arrow. b) The cut is opened up using a bone spreader. c) A fixation plate is screwed in to support the bone as it heals. After surgery, the patient's weight is carried more evenly across both medial and lateral compartments, indicated by the balanced green arrows.

the construct stability and alignment accuracy, as well as increase the healing time and stresses within the fixation plate, leading to plate failure. These effects can result in an unsuccessful treatment.

Previous studies have indicated that the position of the osteotomy cut influences the fracture likelihood by affecting stresses and strains at the lateral hinge [6, 13, 14, 7] and displacement of the cut after surgery [4, 6]. These studies have proposed cut parameters for minimising fracture likelihood, but most have only considered the cut opening procedure and not the stability of the knee construct after surgery. To minimise the likelihood of fracture and surgical complications, a cut position that considers both processes during and after surgery is desirable.

The plate fixation procedure has also been shown to induce significant strains in the bone [15, 16], but there is little information about the effects of individual screws and the order in which they are tightened. A better understanding of how plate fixation affects strains in the tibia would aid in proposing more specific and justified guidance to a surgeon performing MOWHTO. This could have the clinical advantage of reducing the frequency of fracture.

The two research paths followed in this study are therefore 1: finding the best apex location to minimise likelihood of a lateral hinge fracture, and 2: finding the best screw fixation procedure to minimise fracture likelihood and chance of surgical failure if a type I hinge fracture occurred. The project was conducted in collaboration with Joel Melton, a consultant knee surgeon at Addenbrooke's Hospital in Cambridge.

2 Literature Review

2.1 Surgery details

Leg alignment is a pivotal factor for the force distribution in the knee joint [10]. Varus of the knee is characterised by separation of the knees when the ankles are in contact [13]. This results in the mechanical axis of the leg passing through the medial (closer to body) side of the tibiofemoral joint or even missing the joint entirely in extreme cases [17]. The mechanical axis is the axis through which load is carried. In a healthy knee joint, the load is split evenly between the medial and lateral compartments. The varus deformity disrupts this balance, causing the medial compartment to carry much more load than the lateral. MOWHTO surgery aims to decrease the load in the diseased medial compartment [10] and restore an even load distribution by straightening the tibia with respect to the femur. This relieves symptoms and delays the progression of osteoarthritis.

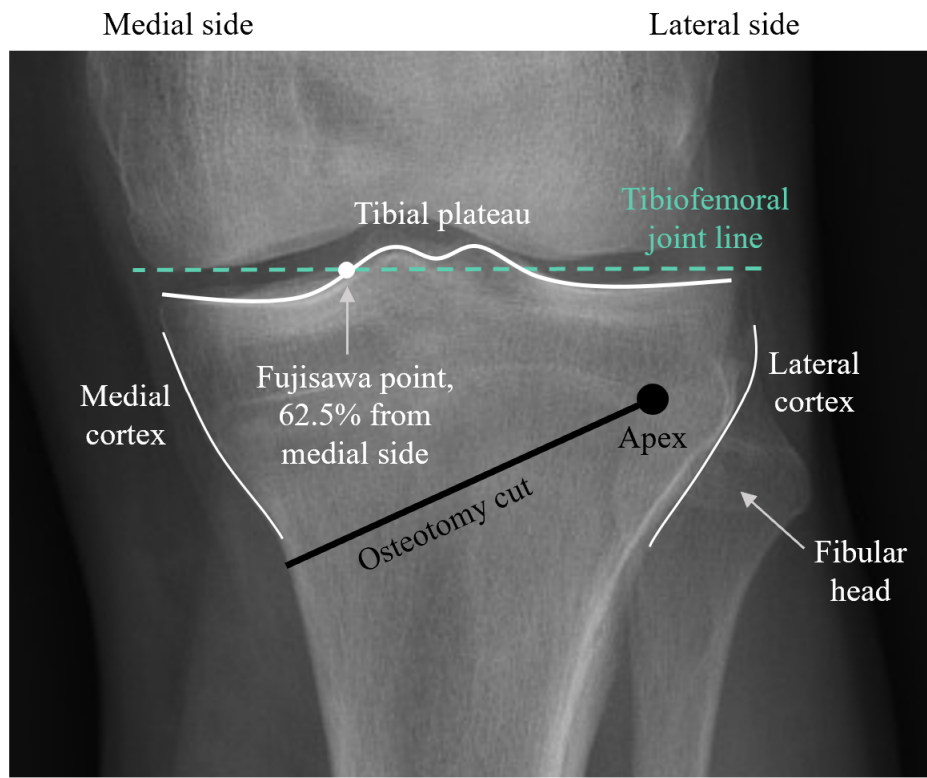


Figure 4: Tibiofemoral joint anatomy and definitions, based on [2].

The alignment of the leg is performed by modifying the tibia geometry. This can be done using the opening wedge technique described in section 1, or using a closed wedge technique where a wedge of bone is removed from the lateral side and the cut is closed [11]. Although the closing wedge method promotes faster healing and allows for larger correction [6, 18] it also presents a higher risk of bone fracture [13]. Hence, this study focuses on the opening wedge method.

The shape and position of the osteotomy cut varies between surgeries. Uni-planar osteotomy is the most standard technique [17] and involves cutting along a single plane. The planar cut is defined by the location of the cut entry point on the medial side and the cut end-point on the lateral side, called the apex. Bi-planar osteotomies involving cuts along two planes are practised less frequently, as they are more complex to perform and have a higher lateral hinge

fracture risk [19]. The cut is usually made by a standard 1.2 mm wide rectangular saw guided by Kirschner wires [6], producing a rectangular cut profile in the coronal plane (figure 5). A strip of bone, known as the lateral hinge, is left intact during cutting to provide stability and enhance healing and bone growth [13]. The cut position has been shown to affect the likelihood of lateral hinge fracture, as described in section 2.3.4)

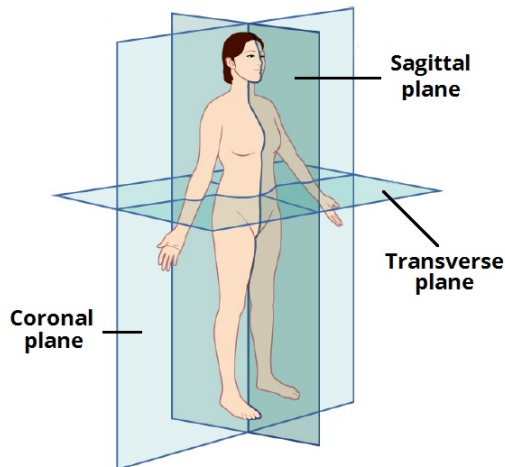


Figure 5: Coronal, sagittal, and transverse plane definition [20].

The angle by which the cut is opened determines the resulting location of the mechanical axis along the joint line. The aim is to shift the axis to the *Fujisawa point* (figure 4), which is 62.5% of the way along the tibial plateau from the medial edge [6]. Correction angles vary between 6 - 15° as it may be beneficial to over or under-correct depending on the patient specific geometry and to account for correction loss [13]. A typical correction angle is 10° which translates to a 10 mm opening of the cut entry [6].

The cut is opened using a chisel or bone spreader [17], and then fixed in place as the support plate is screwed into the bone. The gold standard is the TomoFix™ support plate [21] (see section 2.4). Opening is gradual to encourage toughening of the lateral hinge and reduce the risk of intra-operative fracture (see section 2.3.1). The patient is allowed to bear 30 - 50% [22] of their weight after surgery, depending on the pain and the occurrence of fracture. Full weight-bearing is allowed after two weeks for most patients [23].

2.2 Tibia Bone Material and Mechanics

The tibia is a type of *long bone*, comprised of a hard cortical shell surrounding a spongy trabecular region [24], shown in figure 6.

Cortical bone is made up of bone and collagen fibres in tubular laminate structures called *osteons* (figure 6) [26]. These give the bone increased strength in the longitudinal (along bone axis) direction, creating anisotropic (transversely isotropic in this case) material properties [6, 27]. Multiple osteons are packed together, giving cortical bone its characteristic hard, compact, and brittle nature, and high Young's modulus in comparison to trabecular bone. The cortical bone thickness is on average 3 mm for the proximal tibia, but ranges between 2 - 5 mm throughout the bone [6].

Trabecular bone's mechanical behaviour is less predictable due to its variable, disorganised, and porous structure [27]. It consists of a loose network of bone struts, with gaps filled by blood

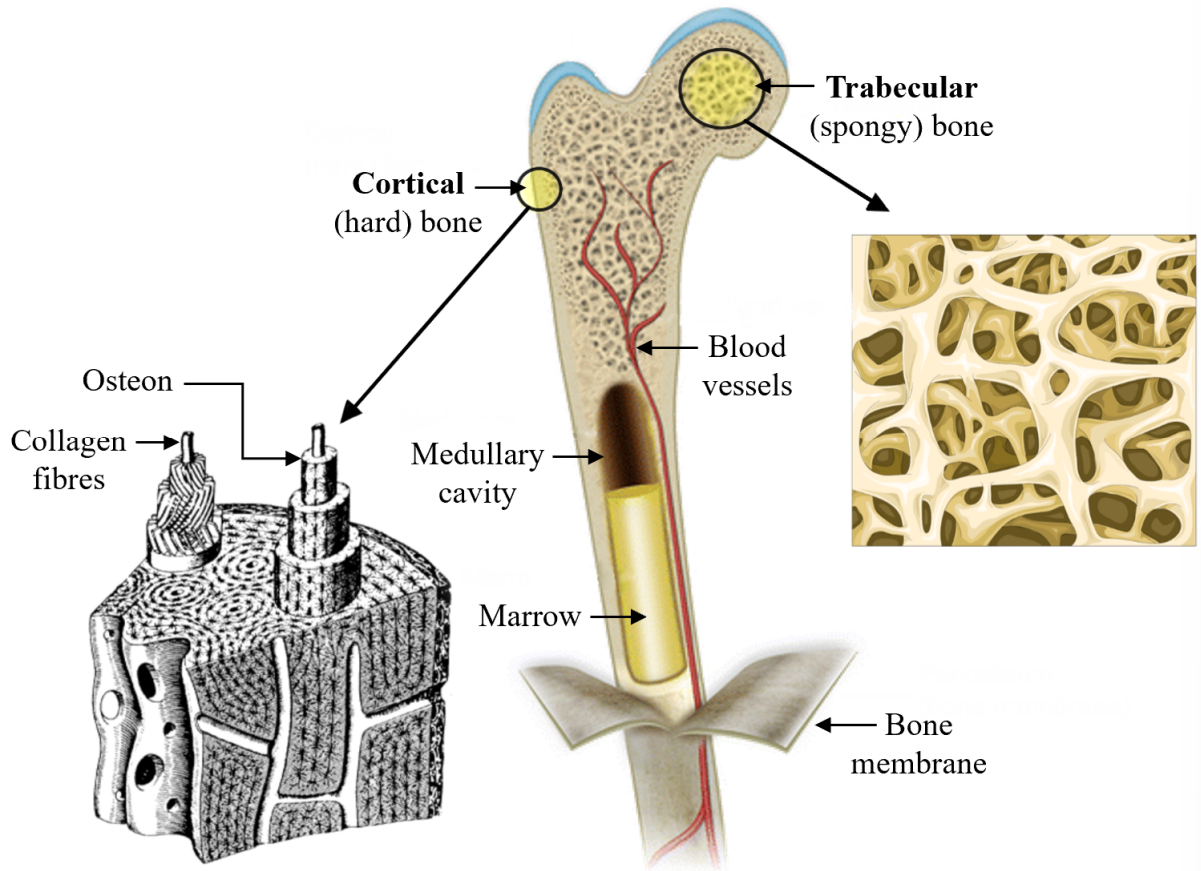


Figure 6: Bone structure, based on [24, 25, 26].

vessels and bone marrow [6]. It is less dense than cortical bone, and has a lower Young's modulus [28].

Bone has a complex range of mechanical properties, as a viscoelastic composite able to repair itself [29]. The mechanical behaviour of bone can be characterised by three regions: elastic, post-yield, and fracture [30]. Material deformations are reversible in the elastic region, but become irreversible post-yield. Cracks form in the fracture region leading to material failure. Model stress versus strain curves for both cortical and trabecular bone in tension and compression are shown in figure 7. The yield point marks the transition between the elastic and post-yield regions, and the ultimate point marks the maximum stress the material can experience before failure. For cortical bone under tension, failure by fracture is rapid after the ultimate point, and the fracture region is almost non-existent.

The post-elastic behaviour of bone is loading-mode dependent [27]. Cortical bone under tension experiences linear hardening post-yield due to collagen fibres bridging microcracks [30]. Under compression, it experiences quasi-brittle softening due to cracks reducing the area under load and hence the strength [30]. It also yields at a much greater stress of 200 MPa than under tension, where it yields around 100 MPa. Trabecular bone softens post-yield under both tension and compression, and its yield stresses are two orders of magnitude smaller than yield stresses in cortical bone.

Cortical bone carries the majority of the total load of the skeleton, and its contribution plays a major role in determining the mechanical properties of a whole bone [29]. However, our present understanding of bone's mechanical behaviour and its multiple constituents is incomplete [27];

finite element simulations and in vitro tests are largely relied on to predict the response of bone to various loads and deformations.

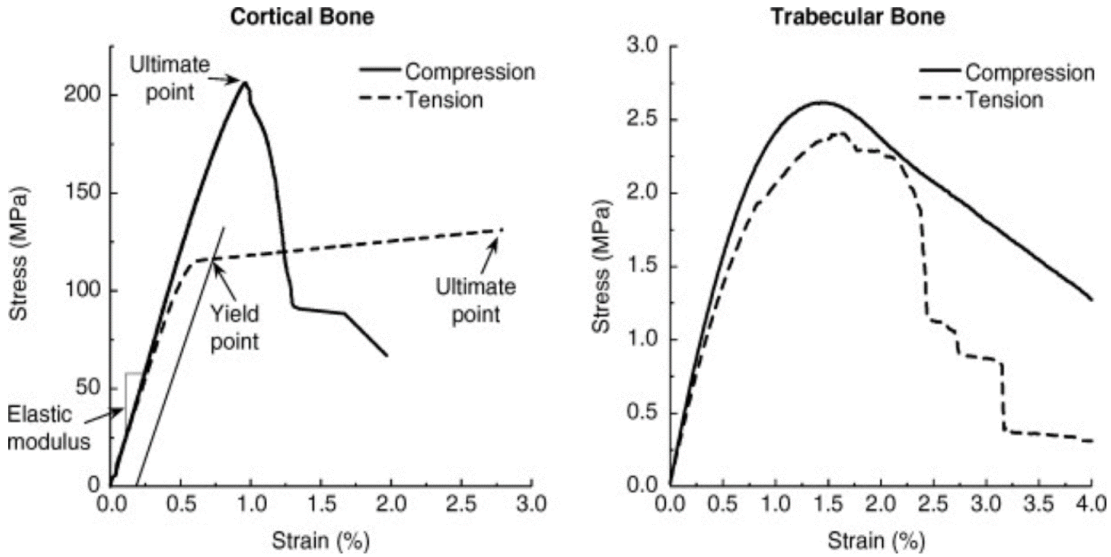


Figure 7: Stress-strain curves for cortical and trabecular bone in tension and compression [31].

2.3 Fracture in High Tibial Osteotomy

2.3.1 Fracture Mechanics

The fracture mechanics of bone are important in the interpretation of finite element results in this study. Resistance to fracture of a bone depends on multiple factors including its mineral content, mineral density, cortical bone thickness, porosity, and crystallinity, and the presence of microcracks [29], but the interplay between these is complex and unclear in places [29]. In general, the prevention of crack growth is more effective in preventing failure than the prevention of crack initiation [29]. Fracture prevention in cortical bone is critical as it provides the most strength and stability for healing, and fails in a brittle manner at smaller strains than trabecular bone [6].

Fractures in bone are studied by measuring the energy required for a crack to propagate and observing the mechanism of fracture through a microscope [33]. Experimental evidence indicates that cortical bone fracture is strain-controlled [34, 32]. The toughening mechanisms in cortical bone during crack propagation are shown in figure 8. Nalla et al. (2005) [34] showed that extrinsic toughening mechanisms (those which act to reduce the crack tip stress intensity) dominate: crack deflection and fibre-bridging. Crack deflection occurs when a propagating crack changes direction after encountering an osteon and takes the path requiring the least energy, parallel to the osteon [6] (figure 8(a)). The stress intensity at the crack tip is subsequently reduced, increasing toughness. Crack-bridging occurs with either uncracked ligaments (figure 8(b)) or collagen fibrils (figure 8(c)) which the crack must cut through to propagate. These mechanisms have similarities with the behaviour of fibre-reinforced composite materials and demonstrate why fracture toughness of bone is anisotropic, with the greatest resistance to fracture in the transverse directions [34].

Microcracking is a toughening mechanism dependent on strain rate [33, 35]. At low strain rates,

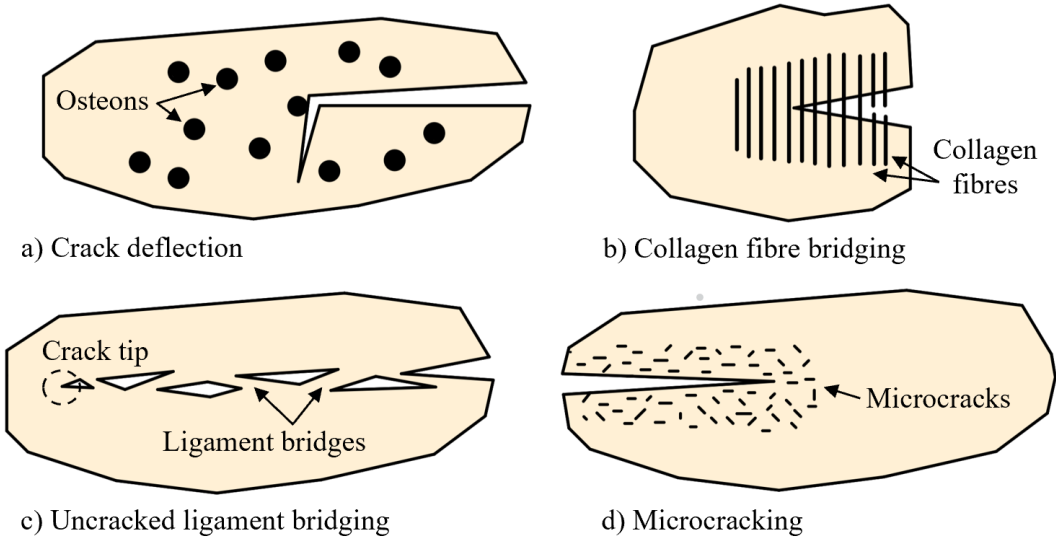


Figure 8: Toughening mechanisms in cortical bone, based on [32]. a) Crack deflection. b) Collagen fibre bridging. c) Uncracked ligament bridging. d) Microcracking.

more microcracks can develop (figure 8(d)), which increase the compliance and hence toughness and fracture resistance of the specimen [35]. Bone has a higher energy for crack propagation at low strain rates compared to most natural materials [33]. At high strain rates, however, bone is brittle and exhibits low toughness. The osteotomy cut is therefore opened as slowly as possible, usually over a period of 10 minutes [6].

Whilst the distribution of strain in cortical bone controls and can thus predict fracture initiation, stress in the bone should be minimised to prevent the material exceeding its yield stress or reaching the ultimate point [6].

2.3.2 Complications and Causes of Fracture

Fractures pose a significant threat to treatment success. They reduce the stability of the lateral side of the tibia, allowing increased movement between the bone regions above and below the cut (termed micromotion) which may cause plate failure, bone non-union, and loss of mechanical axis alignment [6, 7]. Such outcomes would require additional surgery. Frequency of fractures associated with MOWHTO range from 0.3 - 34.0% in literature [16].

Fractures may occur both intra-operatively, during the cut opening and plate fixation processes, and post-operatively, during cycles of gait loading as the patient starts to walk after surgery. A study investigating the complications of MOWHTO in 46 patients (Miller et al. (2009) [36]) found intra-operative and post-operative fracture occurrence to be equally likely. However, some fractures which occur intra-operatively may only be detected a period of time after surgery, as communicated by Mr Melton.

Whilst the cut location and geometry can be controlled to minimise intra-operative fracture likelihood [6, 14], post-operative fracture involves more uncertainty. The gait load and direction vary as the patient moves, and fracture may occur both due to a suboptimal hinge position or lack of plate and screw stability [6]. Kang et al. (2020) [5] suggest that stability can be quantified with values of micromotion, the relative displacement between the upper and lower cut surfaces during loading, shown in figure 9. Excessive micromotion signifies poor construct stability and greater fracture risk, whereas too little may slow down bone healing. Type I and type III fracture

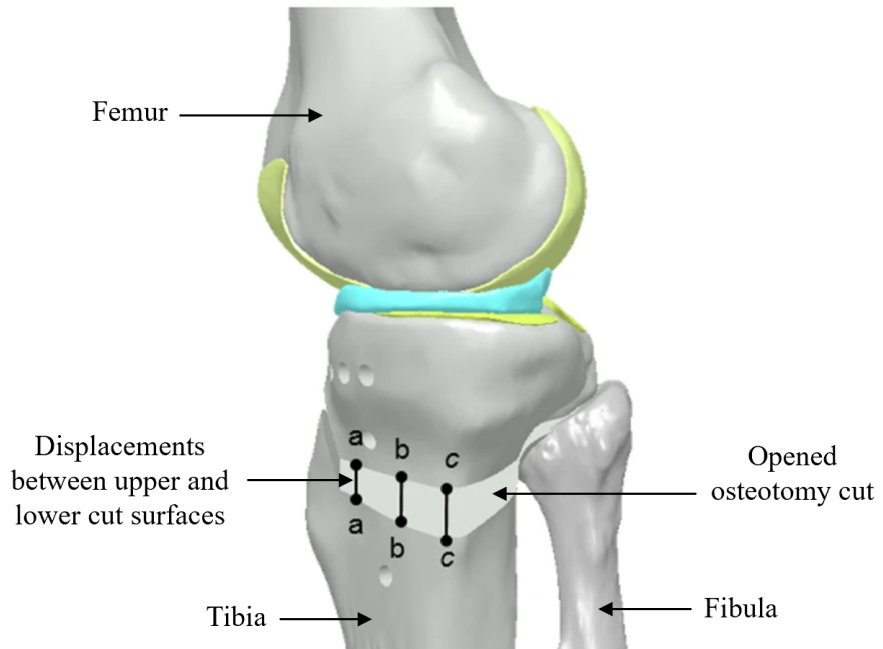


Figure 9: Quantification of osteotomy cut micromotion after MOWHTO, based on [5].

models generally demonstrated micromotion in excess of $200\mu\text{m}$ [5]. An acceptable range of micromotion between $100 - 200 \mu\text{m}$ is proposed by Kang et al. as a rough guideline, but the trade-off between stability and micromotion between cut faces remains unclear.

2.3.3 Fracture Classification

Lateral hinge fractures in MOWHTO can be classified into types I, II, and III, as proposed by Takeuchi et al. (2012) [4], illustrated in figure 10. Type I extends horizontally from the apex to the tibia surface, following the direction of the cut plane. Type II extends down from the apex towards the bottom of the tibiofibular joint. Type III extends up from the apex towards the tibial plateau.

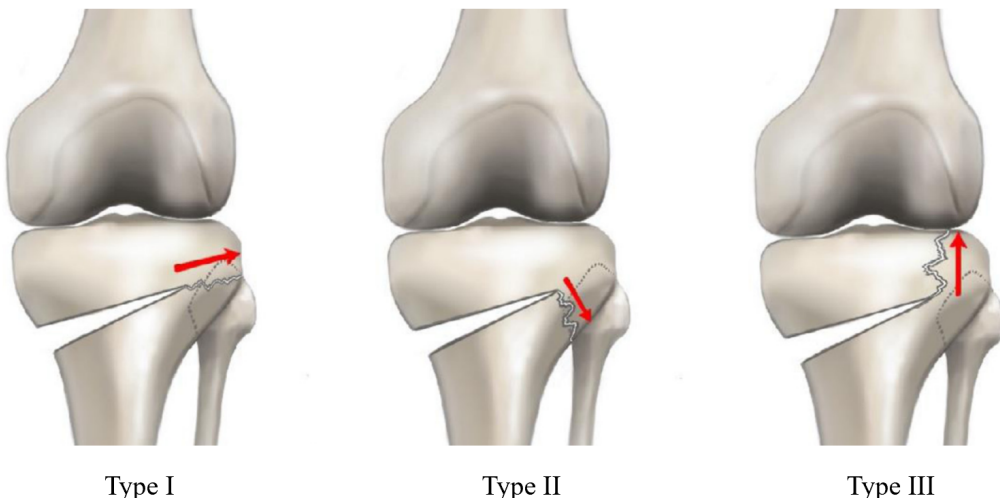


Figure 10: Takeuchi fracture classifications [9]

Fractures vary in frequency and severity according to their type. Type I fractures are the most

common in literature (73% of fractures), and types II and III less common (19% and 8% of fractures, respectively) [7].

Type I fractures are least severe, as weight-bearing post surgery acts to compress the crack, preventing further cracking and enhancing fracture healing [37]. Studies have shown micromotion and gait failure loads for type I fractures and intact hinges to be equivalent [38], and the majority of type I fractures result in no clinical complications [37]. Type II and III fractures are not favourably compressed by weight-bearing, and so exhibit delayed bone union and structural instability. Type III fractures are particularly severe as they create a discontinuity or cleft in the joint surface [7] which will lead to rapid degenerative change within the knee [39]. They often cause over-correction or correction loss [37], and exhibit significantly reduced weight-bearing failure loads and increased micromotion compared with type I fractures and intact hinges [38].

2.3.4 Effect of Lateral Hinge Location

The location of the lateral hinge greatly affects the likelihood and type of intra-operative fracture. A literature review conducted by Earl (2021) [6] identifies common osteotomy cut parameters employed in MOWHTO to prevent fracture. These are summarized in figure 11. The cut entry location is non-critical in fracture prevention and is often 40 mm from the tibial plateau to leave enough bone for inserting proximal screws. Guidance on the lateral hinge width (horizontal distance from apex to lateral cortex) from different studies is contradictory, and there is a lack of consensus across the medical community [13]. Recommended values lie between 5 - 15 mm [14]. The cut apex (end point) should lie within the lateral zone, defined as being lateral to the medial edge of the fibular head [40].

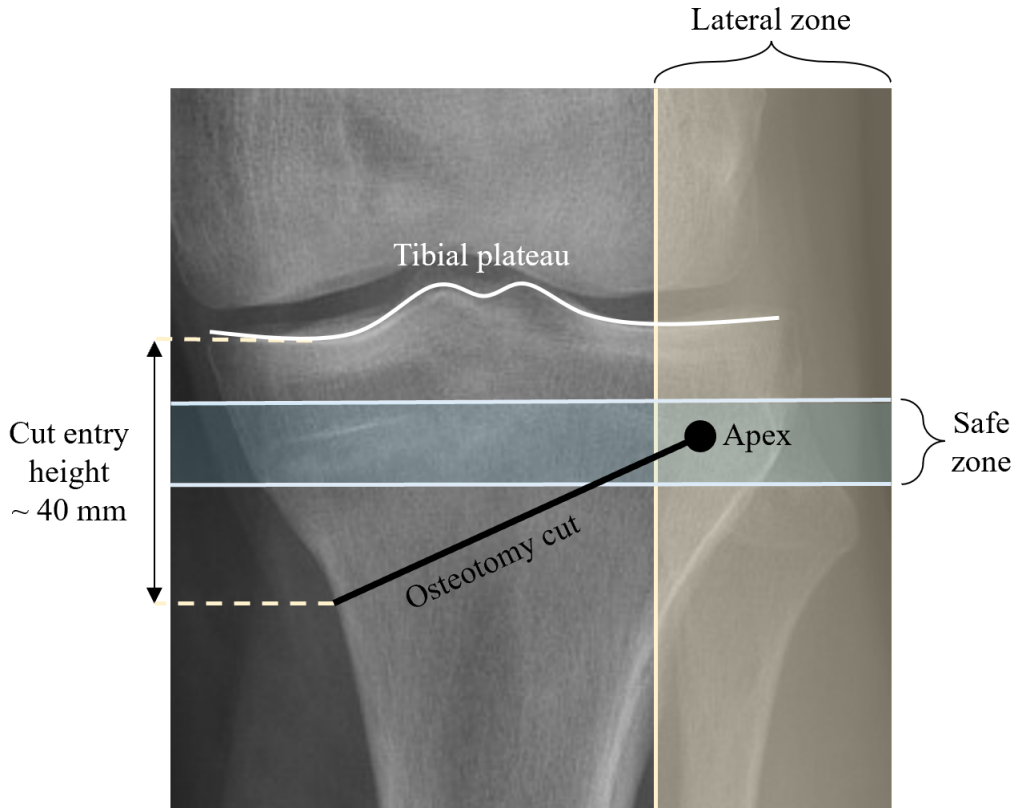


Figure 11: Summary of apex location recommendations from literature, based on [2].

In general, higher apex positions are shown to increase type III fracture likelihood [6, 14]. The height of the fibular head is commonly used as a guide for the osteotomy cut apex position due to increased bone mineral density and fibrous material around it, which improves post-operative stability and bone union [6, 14]. Han et al. (2011) [41] define a ‘safe zone’ for apex height with respect to fibular head height, which reduces fracture likelihood [40, 41, 14]. Apex positions above and below this zone tend to result in type III and II fractures, respectively. As fibular head height varies between patients, other studies propose a set apex distance of 15 - 20 mm from the tibial plateau [40].

Width of the lateral hinge is also shown to affect fracture likelihood; wider hinges of intact bone result in greater strains extending to the tibial plateau and a greater risk of type III fracture intra-operatively [7, 14, 6, 13]. However, narrow hinges are shown to increase micromotion as there is less intact bone to provide stability [6] and an excess of micromotion increases likelihood of fracture post-operatively.

Intra-operative fracture risk and post-operative stability are two competing factors in the search for an apex location which provides the best chance of surgical success. It would be clinically desirable to quantify this trade-off and propose an optimal apex region with minimal complication risk for an average sized tibia, to guide a surgeon performing MOWHTO.

2.4 Plate Fixation Procedure

Various fixation plates are used to support the osteotomy in MOWHTO. The TomoFix plate is used widely as it has better biomechanical properties than other fixation devices [42]. Raja Izaham et al. (2021) [15] showed the TomoFix plate to provide better stability than the Puddu plate through FEA, and Kyung et al. (2015) [43] stated that the TomoFix plate offers a more rigid fixation and early range of motion and weight-bearing. It is the current clinical gold standard for MOWHTO, but there is little investigation into how the sequence used to fixate it affects the stresses and strains it imposes upon the bone.

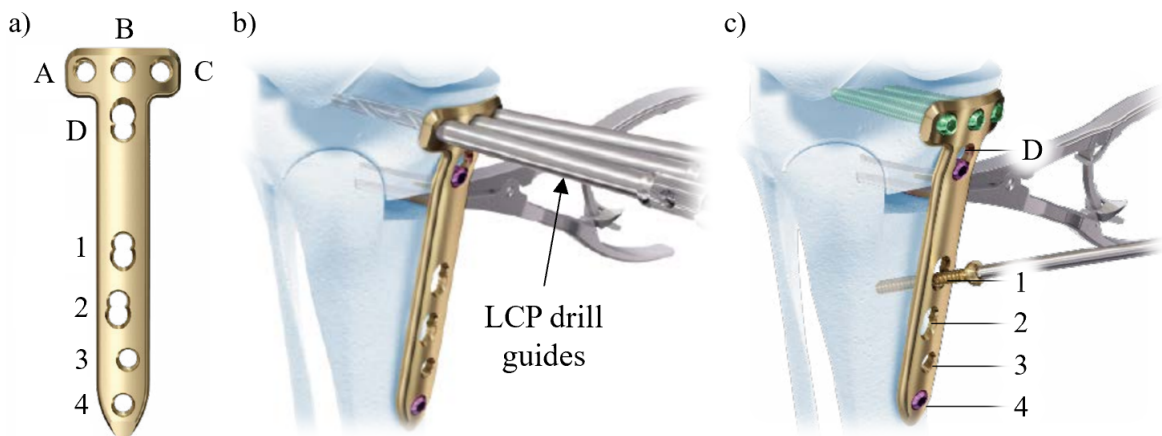


Figure 12: Osteotomy fixation with the TomoFix plate, based on [21]. a) TomoFix hole names for reference. b) Proximal plate fixation. c) Distal plate fixation.

The TomoFix geometry and fixation method is shown in figure 12. First, LCP drill guides are threaded through proximal plate holes A, B, and C (figure 12(a) and 12(b)). The plate is then

positioned against the tibia, ready for fixation. The extent of guidance provided in the TomoFix manual [21] is that the proximal holes must be positioned proximal to the osteotomy gap, 1 cm below the joint line, and the plate's solid midsection should bridge the gap. The top part of the plate head should be parallel to the slope of the medial tibia. Mr Melton explained that the positioning of the plate comes partly through surgical experience and judgement.

The plate is temporarily secured by inserting a Kirschner wire through hole B and the proximal holes are secured with locking screws in the order A, C, then B (green screws in figure 12(c)). To do this, holes are drilled through the bone using a 4.3 mm drill bit guided by the LCP drill guides, followed by the insertion of 5 mm self-tapping locking screws using a power tool, and then full manual tightening using a torque limiter [21]. The screws are chosen to be as long as possible without penetrating the lateral cortex.

Next, the lag screw is inserted into hole 1 in the same fashion as the proximal holes. This screw is a non-locking screw and is inserted temporarily to compress the lateral hinge [21] by bending the TomoFix plate to create an elastic preload. It is replaced by a locking screw once all distal plate holes are fixated. It should be aimed distally, as shown in figure 12(c) so it does not interfere with the path of the locking screw that will replace it. Finally, the distal plate holes are secured with locking screws in the order 2, 3, then 4, the lag screw is replaced with a locking screw, and hole D is secured with a locking screw [44].

Mr Melton presented an alternative method used in surgery, in which the proximal holes are secured with Kirschner wires, allowing rotation between the plate and bone. The lag screw is then partially tightened to begin inducing an elastic preload. Finally, the wires are replaced with locking screws and the lag screw is fully tightened. FE simulations performed by Earl (2021) [6] showed up to a 30% reduction in lateral hinge tensile strains using this method compared to the default method.

3 Project Aims and Structure

This project focuses on fracture prevention and surgical success in MOWHTO. It builds on work conducted on this topic by two previous M.Eng. students, Rosemary Earl [6] and Stanisław Tomaszczyk [13], who used both finite element (FE) and experimental methods to investigate fracture of the lateral hinge. Guidance on the clinical considerations involved and further insight into the surgery was provided throughout by knee surgeon, Mr Joel Melton. A review of existing literature and Mr Melton's experiences as a surgeon helped to identify two important research paths that were followed. The first involved finding the best apex location to minimise likelihood of a lateral hinge fracture. The second involved finding the best screw fixation procedure to minimise fracture likelihood and chance of surgical failure if a type I hinge fracture occurred.

3.1 Optimal Osteotomy Apex Location

Tomaszczyk [13] concluded that wider (larger w) and higher (smaller h) hinges increase type III intra-operative fracture likelihood using a mixture of experimental and FE models. The results were consistent with other literature, but post-operative stability was not considered. Earl [6] considered both intra-operative and post-operative loading to identify an optimal apex region minimising fracture likelihood using finite element analysis (FEA) and a mixture of 2D and sections of 3D models. The study had limitations as the models varied between intra and post-operative analyses and a full 3D analysis was not conducted. The current project

complements the previous work by using a full 3D tibia model consistently across intra and post-operative analyses. We pursue the following research aim:

Aim 1

Find the optimal apex region which reduces the likelihood and severity of fracture both intra and post-operatively, using a 3D tibia model with cortical and trabecular regions consistently across analyses.

3.2 Optimal Plate Fixation Procedure

A literature review and Mr Melton's guidance highlighted the need to better understand the strains at the lateral hinge during plate fixation. Mr Melton suggested that aiming the lag screw distally may reduce tensile stresses at the hinge. He also noted that the reasoning for the commonly adopted top to bottom plate fixation sequence was arbitrary. Earl (2021) [6] showed that Mr Melton's plate fixation method (see section 2.4) reduced axial strains midway across the lateral hinge by up to 30%, but only one alternative sequence was investigated. The current project extends the previous work by conducting a more extensive analysis of different fixation sequences, as well as testing Mr Melton's lag screw angle hypothesis. We pursue the following research aim:

Aim 2

Find the relative strain magnitudes and directions at the lateral hinge during plate fixation.
Investigate how screw insertion order and lag screw angle affects strains.

3.3 Project Structure

The project structure is shown in figure 13. Both experimental and FE approaches were used to investigate the plate fixation procedure to maximise result accuracy.

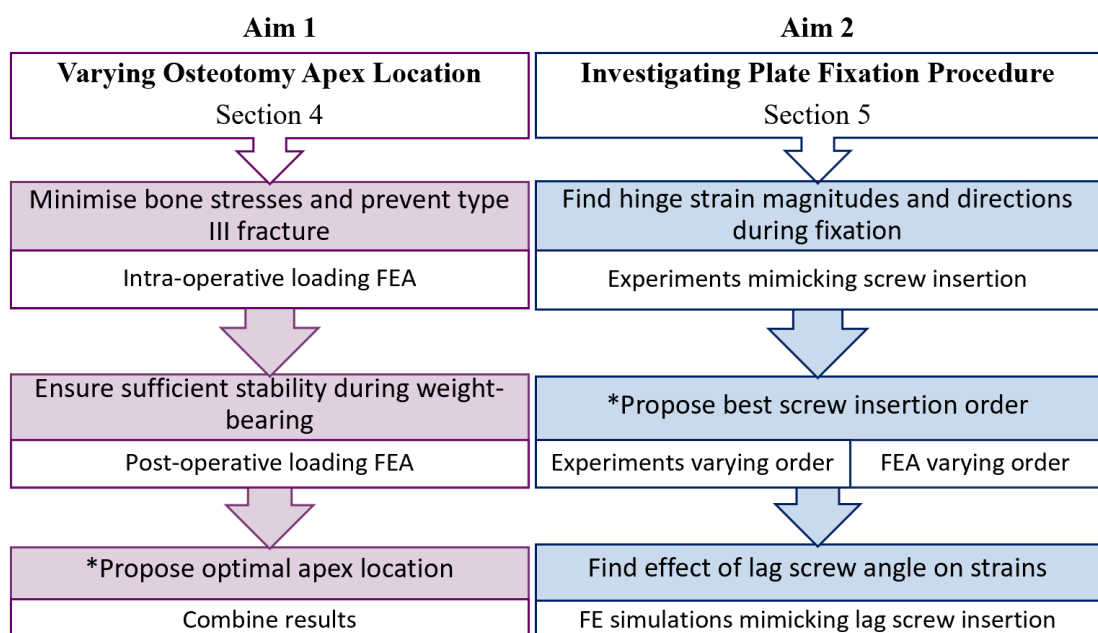


Figure 13: Project structure, * indicates deliverables.

4 Finding the Optimal Osteotomy Apex Location

An optimal osteotomy apex location which minimises surgical risk was found by varying the apex location and observing its effect on fracture likelihood and severity. The problem was tackled by simulating loads incurred during and after surgery, and analysing the stress and strain outputs. Both the intra-operative cut opening process and post-operative weight-bearing were simulated using FEA.

The problem statement is derived in section 4.1. It was important to develop a 3D tibia model for use across all intra and post-operative simulations, described in section 4.2. The methods for this analysis and results derived from intra and post-operative simulations are presented in sections 4.3 and 4.4, respectively. The analysis of these results and their implications for MOWHTO surgery are discussed in section 4.5.

4.1 Problem Definition

The aim of this analysis was to identify an optimal region for the osteotomy apex which minimises the expected surgical risk and hence provides the best expected surgical outcome. The surgical risk $R_{\text{surg.}}$ is a combination of the likelihood of a fracture during or after surgery and the fracture severity.

The osteotomy cut position is fully constrained by the three parameters shown in figure 14: w , h , and h_0 . The lateral hinge width w is the distance from the apex to the lateral cortex, and the apex height h is the distance from the apex to the tibial plateau. These variables define the apex position and form the (w, h) space over which to optimise the apex location. A fixed parameter h_0 defines the cut entry position relative to the tibial plateau. It was set to a constant 40 mm for this analysis, a common cut entry height in MOWHTO and recommended by Mr Melton [6], who noted that the cut entry height h_0 is non-critical for fracture prevention.

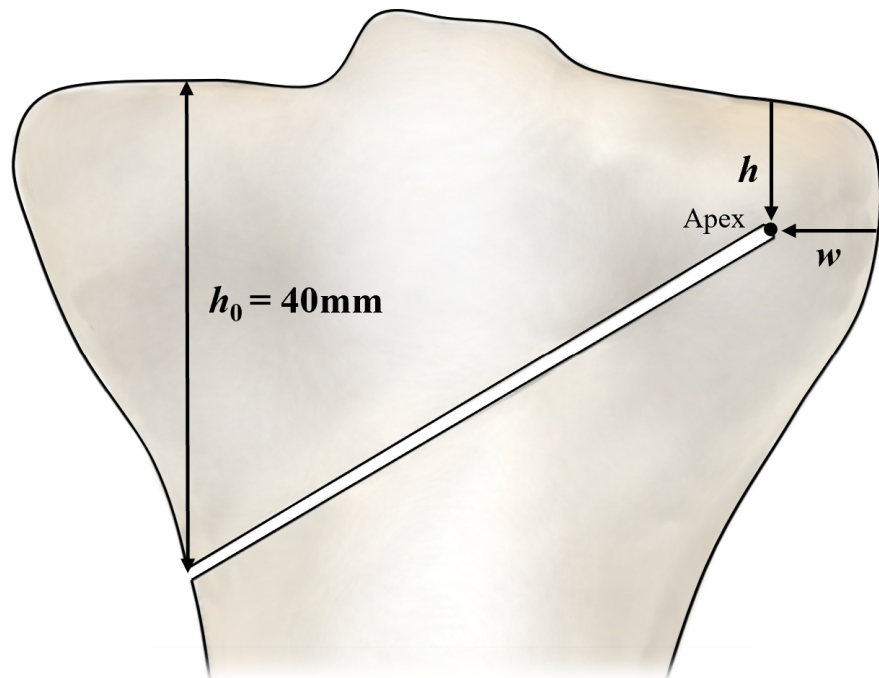


Figure 14: Osteotomy cut parameters. w : width of the lateral hinge, h : vertical distance from apex to tibial plateau, and h_0 : vertical distance from cut entry to tibial plateau.

After fixing h_0 , the problem statement can be formalised as minimising the surgical risk over the (w, h) space, equal to minimising the expected fracture severity. Type II and III fractures are much more severe than type I, but are reported to occur less frequently in literature [16, 7]. Type II fracture predictions were omitted in the following analysis, as an FE study by Earl (2021) [6] and an experimental analysis by Tomaszczyk (2020) [13] on fracture classification at different apex positions showed no occurrences of type II fractures for apex heights less than 20 mm from the tibial plateau. Moreover, Nakamura (2017) [14] found type II fractures to occur in less than 2% of cases, and other studies have indicated them to be associated only with very low apex positions [6], which are excluded by the recommendations in literature. Denoting fracture of type I by T_I and type III by T_{III} , the objective is to find

$$\underset{w, h \in \Omega}{\operatorname{argmin}} (R_{\text{surg.}}), \quad (1)$$

where

$$R_{\text{surg.}} = \mathbb{E}[S|w, h] = \mathbb{P}[T_I] \cdot S(T_I) + \mathbb{P}[T_{III}] \cdot S(T_{III}) \quad (2)$$

$\mathbb{P}[T_I]$ indicates the probability of fracture of type I and $S(T_I)$ is a cost parameter indicating the severity of type I fracture. Omega (Ω) is a set of valid (w, h) configurations, namely, $3 \text{ mm} < w < 15 \text{ mm}$ and $h < 20 \text{ mm}$ from literature [6]. The w and h parameters were defined on a 2D mid-thickness slice of the tibia along the coronal plane, shown in figure 15.

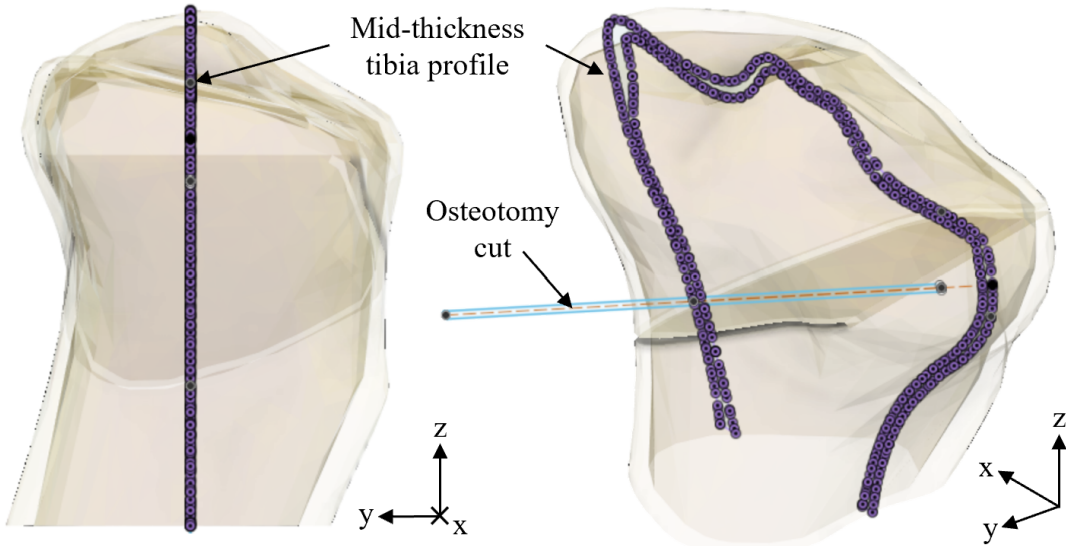


Figure 15: 2D coronal plane tibia profile extracted at mid-thickness to define cut parameters w and h .

Minimisation of the expected surgical risk would ideally be performed by evaluating the expected surgical risk at iterations of (w, h) and performing an optimization procedure such as gradient descent. There is, however, no mathematical model at present for evaluating surgical risk of a lateral hinge fracture, so the optimisation problem is tackled with a simplified approach.

Is it reasonable to assume from the trends seen in literature [6, 14] that the expected surgical risk has a single minimum over (w, h) in Ω . Hence, a subset of (w, h) space can be found in which the minimum will lie by considering intra-operative and post-operative processes separately, and by eliminating regions of (w, h) space to align with appropriate criteria.

Objective

Find the subset of (w, h) space, $F \subset \Omega$, such that

$$\underset{w, h \in \Omega}{\operatorname{argmin}} ([R_{\text{surg.}}]) \in F \quad (3)$$

Intra-operative analysis focused on distinguishing apex regions for which type III fractures were more likely than type I and eliminating these regions due to the high severity of type III fracture compared with type I. Post-operative analysis focused on eliminating apex regions for which micromotion during weight-bearing lay outside the acceptable 100 - 200 μm range [45]. Both streams of analyses were combined, along with the aforementioned bounds from literature, to produce a locus in (w, h) defining the optimal apex location for surgical success.

4.2 Tibia model used in intra and post-operative analyses

The tibia was modelled by a simplified representation of a real tibia bone for speed of FE simulations. A dense proximal tibia surface mesh was extracted from a patient knee CT scan¹ (figure 16(a)). The CT data was provided by Dr Segal (University of Kansas Medical Center) with the help of Dr Turmezei (Norfolk and Norwich University Hospitals NHS Foundation Trust). The tibia was chosen due to its average size from a set of bones appropriate for MOWHTO. The distal tibia was removed from the mesh and replaced with an encastre (fixed) boundary condition in all subsequent analysis, as this region remains a fixed rigid body during surgery and is far enough from the lateral hinge and osteotomy cut (the regions of interest) to be assumed independent of these.

The range of Young's moduli in real bone are often modelled by two discrete cortical and trabecular sections in FE simulations and biomechanical analyses for speed and practicality [15, 5, 46, 47]. These bone regions are often assigned linear elastic and homogeneous properties as an approximation. The mesh was processed in Fusion 360 by decimation and splitting to produce two distinct bone regions, an inner trabecular region surrounded by a cortical shell region (figure 16(b)). A 0.5 mm tolerance (maximum deviation of vertices from their starting position) decimation was employed consistently across all meshes with varying osteotomy cut geometry to ensure all objects were decimated to the same accuracy. The applied 0.5 mm tolerance was valid, as this value is smaller than the ± 2 mm accuracy of the surgical saw used to create the osteotomy cut.

Material properties were assigned using parameters in Kang et al. 2020 [5], shown in table 1. Cortical bone was assigned transversely isotropic properties, with identical properties in the x and y directions, and different properties in the z (vertical) direction, along the bone's longitudinal axis. In contrast, trabecular bone was assigned isotropic properties. Both cortical and trabecular bone regions were modelled as homogeneous linear elastic materials, neglecting plasticity and viscoelasticity for speed and ease of analysis, as done in Kang et al. (2020) [5]. Stress and strain magnitudes were not numerically representative of the physical reality due to these simplifications, but were comparable between simulations nonetheless and were adequate to obtain cut geometry which minimised the cost function.

¹Use of the CT data for the bone studied in this project was approved under the KUMC Policy for Flexible IRB Review, IRB: STUDY00146751. The Approval of Submission document is given in Appendix C. All images were anonymised.

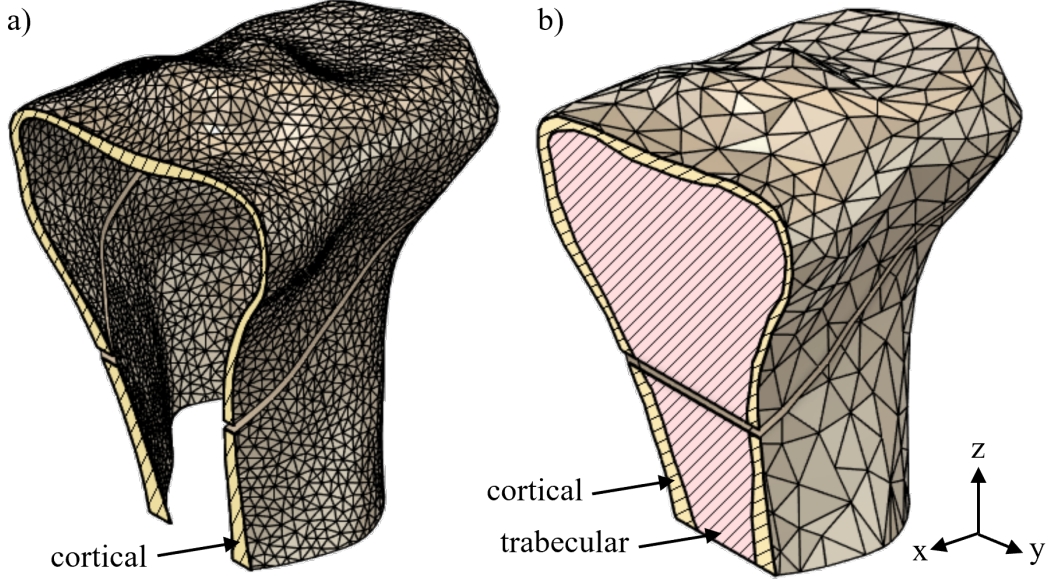


Figure 16: Section views of proximal tibia meshes derived from patient CT scan. a) Original dense mesh, solely consisting of cortical bone. b) Decimated mesh, consisting of cortical shell and trabecular inner solid.

Table 1: Cortical and trabecular bone material properties used in simulations, based on [5]. E = Young's modulus, G = Shear modulus, and ν = Poisson's ratio.

Material	Type	E_x/E_y (GPa)	E_z (GPa)	G_{xy} (GPa)	G_{xz}/G_{yz} (GPa)	ν_{xy}	ν_{xz}/ν_{yz}
Cortical bone	Transversely isotropic	11.5	17	3.6	3.3	0.51	0.31
Trabecular bone	Isotropic	2.13	2.13	-	-	0.3	0.3
Titanium plate	Isotropic	110	110	-	-	0.3	0.3

4.3 Intra-operative Analysis

4.3.1 Methods

The osteotomy cut opening process during surgery demands the greatest displacement of the osteotomy cut and induces significant stresses in the bone. Tomaszczyk (2020) [13] showed cut opening to cause type I and III fracture in Perspex tibia models and identified a pattern between fracture nucleation location and fracture type (see section 4.3.2). Since fracture type III severity is much greater than type II, $S(T_{III}) \gg S(T_I)$ (equation 2), the goal becomes minimization of $\mathbb{P}[T_{III}]$ (type III fracture probability).

The osteotomy cut opening surgical procedure was simulated in Abaqus with the setup depicted in figure 17(a). An encastre (fixed) boundary condition was imposed on the bottom surface as described in section 4.2. A 10 mm vertical displacement (in the positive z direction) was applied to a reference point at the osteotomy cut entrance, corresponding to the 10° osteotomy correction angle typical in surgery [6]. The motion of a set of nodes in the local vicinity of the cut entrance was constrained to the motion of the reference point, forcing them to move together as a rigid body to prevent a stress singularity [48]. The tibia geometry was modified between simulations to vary hinge width w and height h .

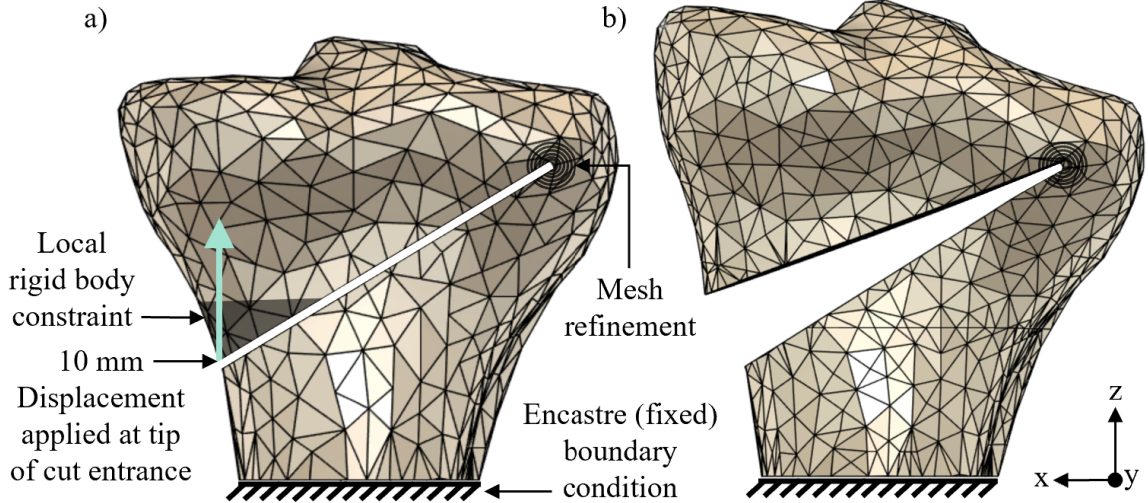


Figure 17: Intra-operative model labelled with boundary conditions and constraints. Upwards displacement applied at the cut entrance to mimic cut opening, and nodes in the vicinity of applied displacement point constrained to move as a rigid body.

The maximum stresses and largest stress and strain gradients occurred at the apex in initial intra-operative simulations. Hence, the FE mesh used in these simulations was refined around the apex to improve accuracy of the output stress and strain maps.

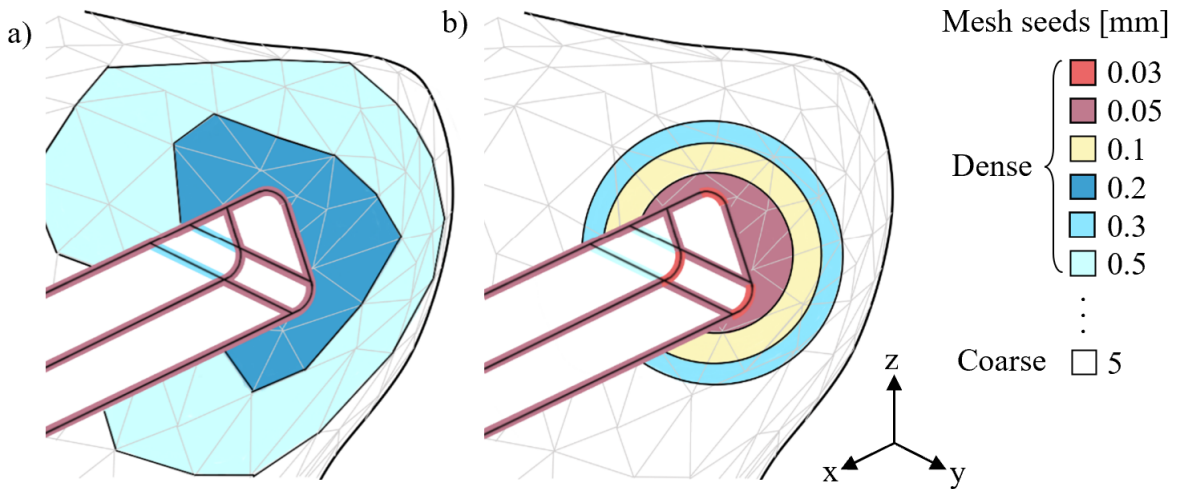


Figure 18: Local mesh seed settings at apex region (in mm); global seed spacing is 5 mm. a) Reference mesh with large apex refinement. b) Mesh used in intra-operative simulations. Diagram not to scale.

Nine different sets of mesh seeding constraints were analysed to find an optimal set of seeding constraints which maximised output accuracy (ideally within 5% of a high accuracy reference) whilst keeping simulation duration under a practical limit of thirty minutes. In addition, a reference simulation was run with a large dense region extending 10 - 20 mm around the apex and the set of seed constraints shown in figure 18(a). It took four hours to run and was used to assess the accuracy of coarser meshes.

The set of seeding constraints chosen for intra-operative analysis is shown in figure 18(b), with 5 mm global seed spacing. Seed spacing across the tibia varied between 0.05 - 5 mm, comparable to the 0.2 - 5 mm spacing used in a linear elastic FE study of tibial osteotomy cut opening in

Kaze et al. (2017) [45] and 1 - 4 mm spacing used in Bostrm et al. (2020) [7]. Seed spacing constraints were applied on a series of concentric circles centred at the apex, the largest with a 2.5 mm radius, to ensure FE mesh consistency across different osteotomy cut geometries. The resulting graded mesh was fine near the apex, and gradually coarser moving away from the apex. Intra-operative simulations took up to thirty minutes to run with this mesh, using quadratic finite elements, and maximum stress values for two different cut geometries deviated from their respective reference simulation values by up to 2%.

4.3.2 Fracture Type Classification

Prediction of fracture type after each intra-operative simulation was done either by observing the pattern of strain magnitudes around the apex or by observing the location of the highest strains around the apex edge. Earl (2021) [6] used the former method, which worked well for FE meshes that were dense around the whole shoulder of the lateral tibia. The latter method was inspired by Tomaszczyk's findings [13] and only required inspection of the strains in the local apex vicinity and hence a dense mesh here. Both methods complement the experimental evidence that the onset of fracture in cortical bone is strain-limited (section 2.3.1).

Earl's fracture classification method [6] relied on observing the pattern of strains across the lateral tibia shoulder, depicted in figure 19. Type I fracture was predicted when high strains stretched across from the apex to the lateral cortex, and type III fracture was predicted when high strains stretched up from the apex to the tibial plateau. Strain patterns indicating type II fracture were not observed in any of the simulations.

Tomaszczyk found all type I fractures to nucleate at the lower apex corner and type II fractures at the upper apex corner [13], demonstrated in figure 19. This translated in FEA as higher strains in the lower corner predicting a type I fracture, and higher strains in the upper corner predicting a type III fracture:

$$\frac{\varepsilon_{upper\ corner}}{\varepsilon_{lower\ corner}} \propto \frac{IP[T_{III}]}{IP[T_I]} \quad (4)$$

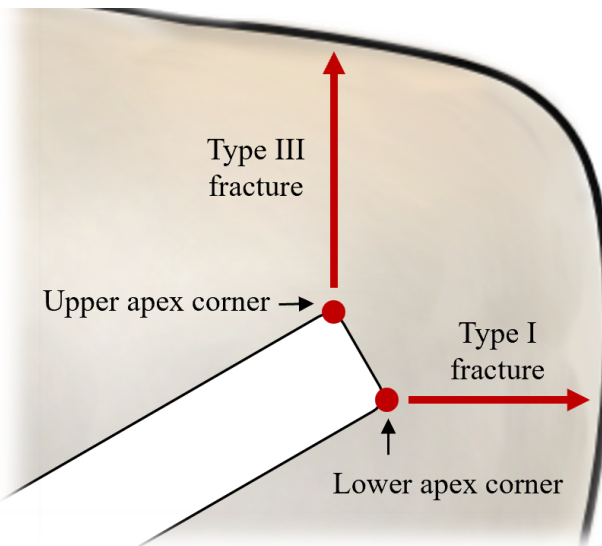


Figure 19: Fracture classification by location of strain nucleation, based on results by Tomaszczyk [13]. The region of bone shown is the lateral tibia shoulder. Type I fractures nucleate at the lower apex corner and type III at the upper apex corner.

4.3.3 Results and Discussion

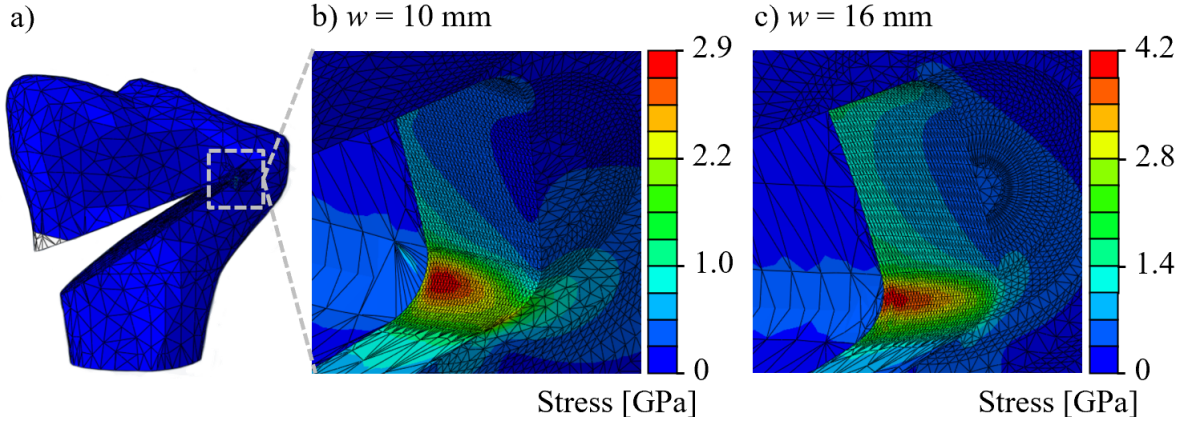


Figure 20: Stresses at the apex after cut opening simulations for hinge height $h = 12$ mm. a) Deformed geometry from FE simulation output. b) Stresses for $w = 10$ mm. c) Stresses for $w = 16$ mm.

The maximum von Mises stress in the tibia occurred through the thickness of the cortical bone at the lower apex corner for all intra-operative simulations and ranged between 1 - 5 GPa, matching the order of 2 GPa in an FE study by Kaze et al. (2017) [45]. The stresses at the apex for hinge height, $h = 12$ mm, and two different hinge widths, $w = 10$ and 16 mm, are shown in figure 20. Maximum stress was greater for the wider hinge and stress contours are smooth, indicating adequate mesh refinement.

Variation of maximum stress in the tibia with the lateral hinge width at a constant hinge height of 8 mm is shown in figure 21(a). Blue data points indicate predicted type I fracture, and red data points type III fracture, by classification using location of strain nucleation (section 4.3.2). Figures 21(b) to (d) show strains around the apex for $w = 6, 8$, and 16 mm, respectively, to demonstrate how fracture type was identified. Where strains were greatest at the lower apex corner (figure 21(b)), a type I fracture was predicted, and type III where strains were greatest at the upper apex corner (figure 21(d)). Where strains nucleation at the upper and lower apex corners appeared to be equal (figure 21(c)), the data point was labelled with type III fracture, as this was the most severe possibility out of the two equally likely fracture types. Additional simulations were run with elastic-perfectly plastic material properties for four different cut geometries, and fracture classification consistently matched that of the corresponding elastic analysis.

Maximum stress increased with hinge width for $h = 8$ mm, and similarly for simulations at all hinge heights. The increase was more gradual for smaller w and type I fracture, and more rapid for larger w and type III fracture. As a first order approximation, the relationship between w and maximum stress was modelled by two lines of best fit with differing gradients. The point of intersection of these lines was estimated to be the hinge width which gives equal likelihood of type I and type III fracture, synonymous with a type I to type III transition location. Similar trends were observed for different h values between 7 - 11 mm (table 2, Appendix A), with the type I to type III transition point shifting to a larger w value with increasing h . The type I to III transition hinge width was found for multiple hinge heights, and a Line of Best Fit was plotted in figure 23 (blue line), giving a bound in (w, h) to avoid type III predicted fracture: $h > 0.26w + 6.2$.

This analysis was repeated using the wider strain image fracture classification method (section 4.3.2). In this method, high strains across the lateral shoulder of the tibia which stretched

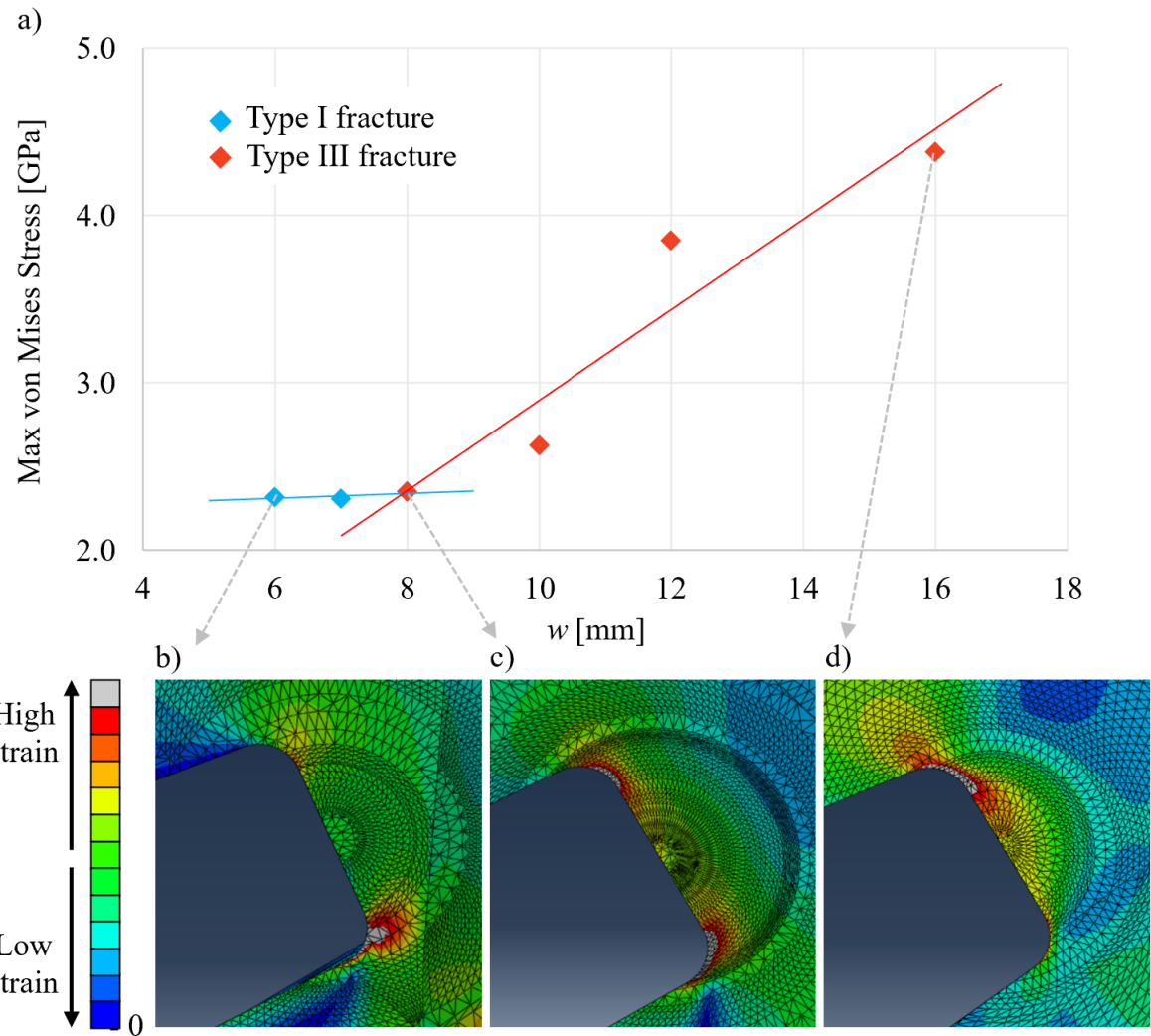


Figure 21: a) Variation of maximum stresses at the apex with lateral hinge width for hinge height $h = 8$ mm. b) Apex strains showing type I fracture for $w = 6$ mm. c) Apex strains showing type I or type III fracture for $w = 8$ mm. d) Apex strains showing type III fracture for $w = 16$ mm.

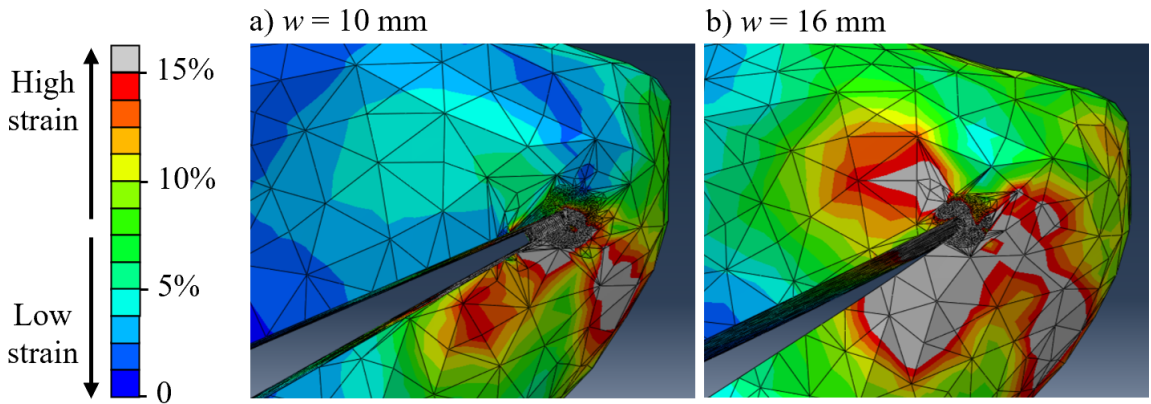


Figure 22: Wider strain images for $h = 12$ mm and $w =$ a) 10 mm and b) 16 mm. Alternative fracture classification method.

from the apex to the lateral edge of the bone (figure 22(a)) were taken as predicting type I fracture, and high strains stretching up from the apex towards the tibial plateau (figure 22(a)) were taken as predicting type III fracture. The (w, h) bound to prevent type III fracture using the wide strain image fracture classification method is shown as the purple line in figure 23: $h > 0.65w + 4.1$.

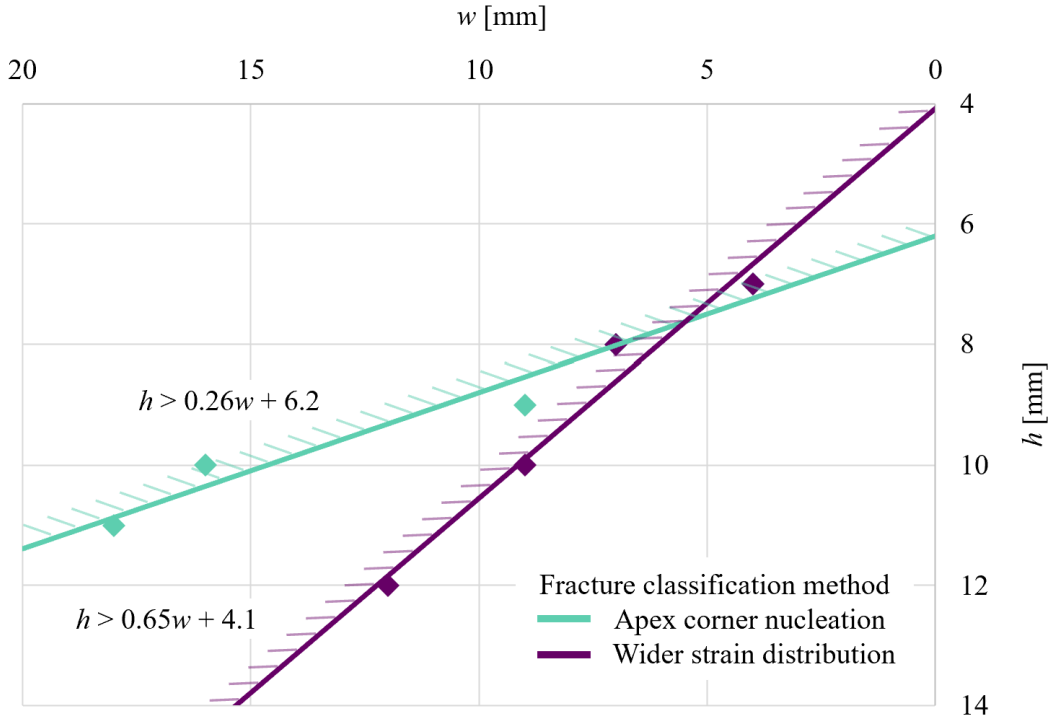


Figure 23: Predicted type I to III transition bounds for two different fracture classification methods.

The most appropriate fracture classification method of the two considered is unknown. Although the strain-limited behaviour of cortical bone fracture supports the wider strain distribution method, the finite element mesh may have been too coarse around the lateral tibia shoulder for an accurate evaluation using this method. Meanwhile, comparing the strains at the upper and lower apex corner to predict fracture type, as suggested by Tomaszczyk (2020) [13], was an experimentally derived classification method with uncertainties in translating its use to FEA. Hence, a third ‘worst case’ bound was estimated for preventing type III fracture, representing the most conservative of the figure 23 bounds for each hinge width: $h > 0.56w + 6.0$. This bound was used when proposing an optimal apex region in section 4.5.

Summary: Intra-Operative Analysis

Narrow lateral hinge widths and those closer to the tibial plateau increase the likelihood of a type III fracture.

Fracture classification can be performed using the corner of strain nucleation at the apex or the wider strain distribution. Bounds in (w, h) for apex locations preventing type III fracture are $h > 0.26w + 6.2$ for the strain nucleation classification method, and $h > 0.65w + 4.1$ for the wider strain classification method. All units are measured in mm.

A ‘worst case’ bound is estimated for use in proposing an optimal apex region: $h > 0.56w + 6.0$.

4.4 Post-operative Analysis

During post-operative weight-bearing, the tibia, plate, and screw construct must withstand large loads with limited displacement. Kang et al. (2020) [5] devised a method of quantifying the construct stability using values of micromotion, the displacement between the upper and lower cut surfaces, as described in section 2.3.2. It was suggested that micromotion should be between 100 - 200 μm for good stability, yet enough movement to trigger timely healing of the cut. Weight-bearing FE simulations were conducted to obtain trends between apex location and micromotion, and determine an apex region which keeps micromotion within the proposed limits.

4.4.1 Methods

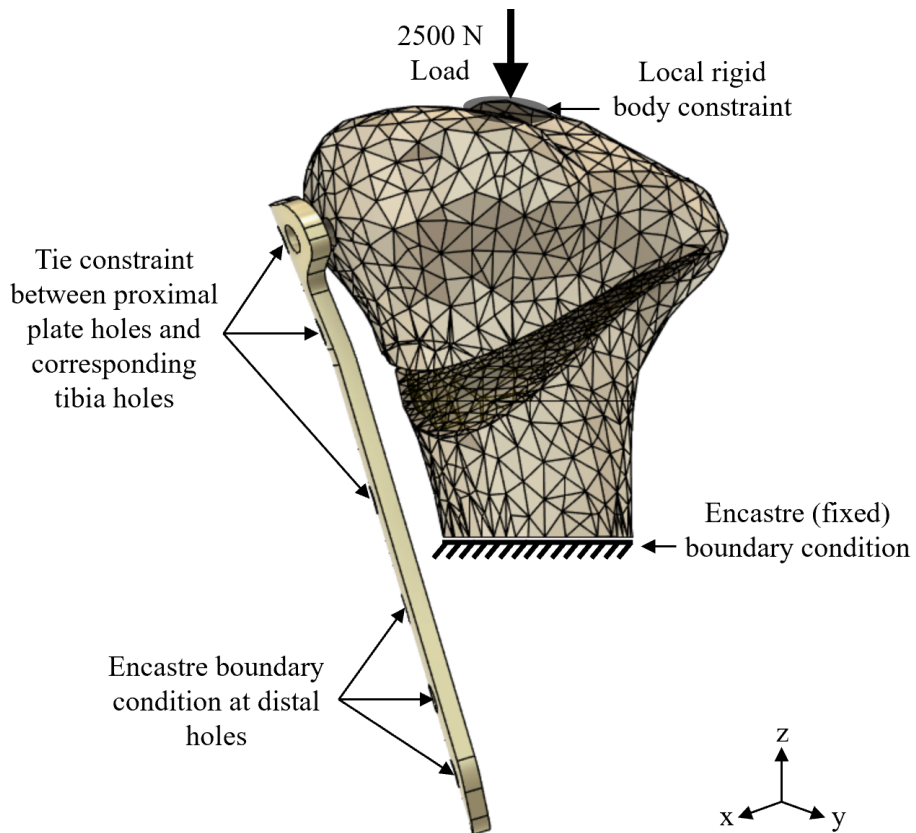


Figure 24: Post-operative model with labelled boundary conditions and constraints. Downwards load applied through centre of tibial plateau to mimic weight-bearing, and nodes in the vicinity of applied load point constrained to move as a rigid body.

Load through the knee joint during weight-bearing was simulated in Abaqus with the setup depicted in figure 24. An encastre (fixed) boundary condition was imposed on the bottom surface as described in section 4.2. A 2500 N load, corresponding to 3.1 times the body weight of a patient weighing 80 kg, was applied to a reference point at the highest point on the tibial plateau to represent the maximal axial force during the gait (walking) cycle [5]. It was applied in the negative z direction, along the bone's longitudinal axis, as an estimate for the patient's weight-bearing axis. The motion of a set of nodes in the local vicinity of the reference point was constrained to the motion of the reference point, forcing them to move together as a rigid body to prevent a stress singularity [48]

Tie constraints were imposed between the proximal plate holes and corresponding tibia holes to

model the constraints between these features imposed by the rigid locking screws during surgery. The distal plate holes were fixed in place by an encaustre boundary condition as these lay below the proximal tibia model and were assumed fixed by continuation of the tibia encaustre boundary in the x-y plane.

The mesh used in post-operative simulations was coarse because interest was in the rotation of the upper cut segment towards the lower cut segment, modelled as two rigid bodies joined at the lateral hinge. There was no apex refinement, since accurate stress and strain values were not required.

Micromotion was quantified by measuring the relative displacement of the upper and lower cut surfaces along three different vertical lines near the cut entry, as in section 2.3.2 [5], and averaging these values. The same six geometrical points were used across all tibia geometries, with varying lateral hinge width and height.

4.4.2 Results and Discussion

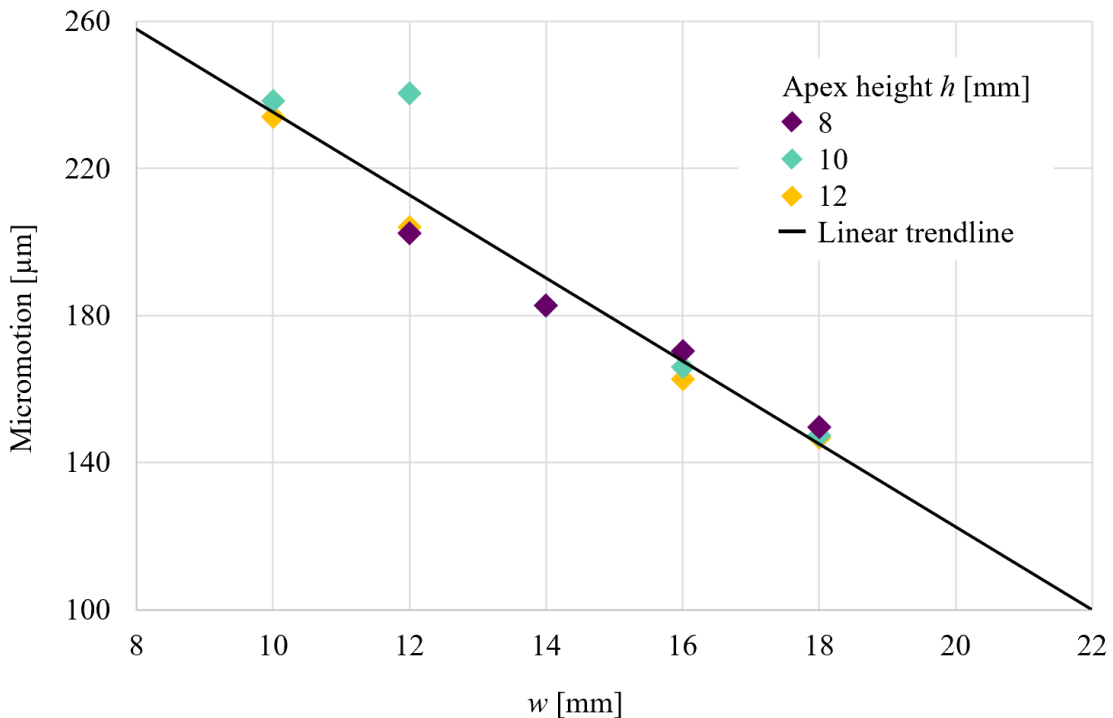


Figure 25: Micromotion averaged over three locations at the cut entry with varying hinge width for three different hinge heights.

The micromotion at different lateral hinge widths for three different hinge heights is shown in figure 25. Micromotion decreased with increasing hinge width, as expected, since wider hinges have more intact bone to provide stability and reduce cut displacement. On the contrary, micromotion remained relatively constant across different hinge heights. A linear relationship between hinge width and micromotion can be approximated, as shown by the black line in figure 25. This trend predicts that w should be between 13 - 22 mm for micromotion between 100 - 200 μm .

It is important to note that placement of the fixation plate against the tibia affects the amount of micromotion. A study by Luo et al. (2015) [49] found that positioning the plate anteriorly,

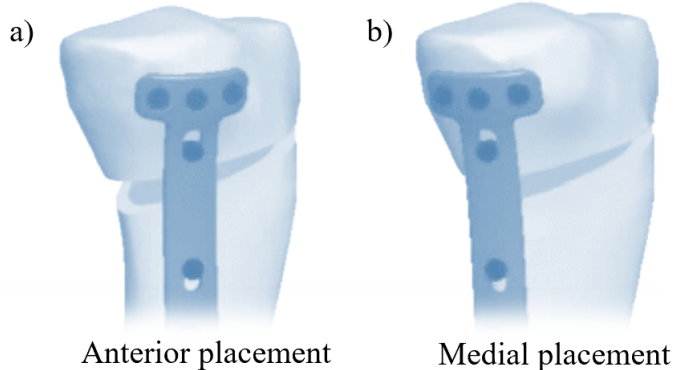


Figure 26: Fixation plate placements in MOWHTO. a) Anterior placement. b) Medial placement.

towards the front of the body (figure 26(a)), versus medially, towards the medial side and closer to cut entry (figure 26(b)) had different effects on stability. Anterior placement gave lower stiffness, more micromotion, and smaller failure loads than medial placement. The setup used in post-operative analysis in this investigation (figure 24) had anterior plate placement. If the plate was shifted medially, closer to the cut entry, there would likely be less micromotion for the same hinge widths. This suggests that 13 mm lower bound on w is non-strict and depends on plate positioning. It would be beneficial to be closer to this bound than the higher 22 mm bound, as it is likely to be in the region of overlap for acceptable micromotion with both anterior and medial plate placement.

Earl (2021) [6] found micromotion to have some dependence on lateral hinge height in post-operative analysis and proposed a (w, h) bound for acceptable micromotion: $h < -2.4w + 34$. The model used for simulations differed significantly from the model presented here, which may explain the difference in trends found. Earl used a 2D fully cortical tibia model, in contrast to the 3D model with cortical and trabecular bone regions used in this analysis. A different patient's knee was used for geometry creation compared to the patient knee of average size used here. Earl positioned the plate medially as opposed to anteriorly, shedding light on the less conservative lower bound found for the hinge width.

Summary: Post-Operative Analysis

Narrow hinges cause more micromotion, reducing post-operative stability, and wide hinges cause slow healing.

Bounds of $w > 13$ mm and $w < 16$ mm can be given for the apex position to keep micromotion between 100 - 200 μm , with the lower bound being loose due to anterior plate placement.

4.5 Surgical Implications

Results from intra-operative and post-operative analyses were combined to propose a closed bound on ω , the space in which the optimal apex location is thought to lie. Aiming the apex in this space minimises the expected surgical risk and, hence, the chance and severity of fracture and surgical complication.

The proposed apex region which minimises expected surgical risk is given as a locus in figure 27. An intra-operative ‘worst case’ contour in (w, h) for predicted type I to type III fracture transition was estimated from the two contours derived using different fracture classification methods in

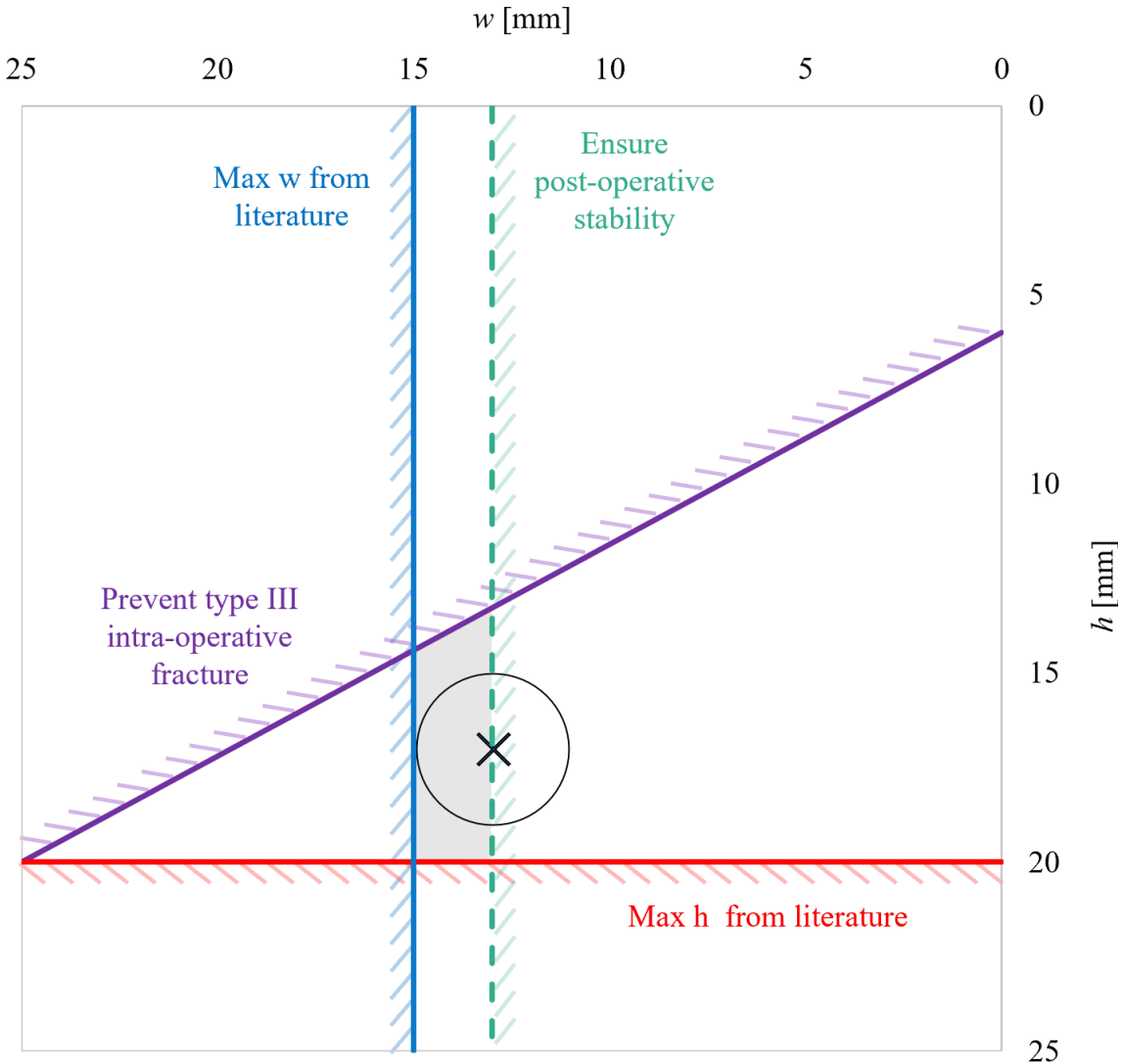


Figure 27: Proposed region for the osteotomy apex from the concatenation of (w, h) bounds, indicated by grey shading. Optimal location marked by X is at $w = 13$ mm, $h = 17$ mm, with a 2 mm radius circle to represent the accuracy of the saw cut. Hatching indicates areas which do not satisfy the proposed inequalities.

section 4.3.3. The $w > 13$ mm bound to prevent micromotion greater than $200 \mu\text{m}$ was imposed as a loose bound, as it is an overestimate of the hinge width to ensure post-operative stability, due to anterior plate placement (section 4.4.2). Bounds of $w < 15$ mm and $h < 20$ mm were imposed from literature.

An optimal apex position of $w = 13$ mm, $h = 17$ mm is suggested, marked by an X in figure 27. This was calculated by taking the centroid of the grey region, then imposing a strong bias towards $w = 13$ mm, as this bound is non-strict and likely over-conservative. A 2 mm radius circle surrounds the optimal point to represent the 2 mm accuracy of the saw cut due to the flexibility of the saw-blade [6]. The proposed hinge width lies within the 5 - 15 mm quoted in literature [14]. The hinge height lies within the 15 - 20 mm range quotes across literature. An average apex position from recommendations given in literature is $w = 9.5$ mm, $h = 18.5$ mm. The optimal points proposed in this analysis and recommended from literature are similar in hinge height, and differ more in hinge width.

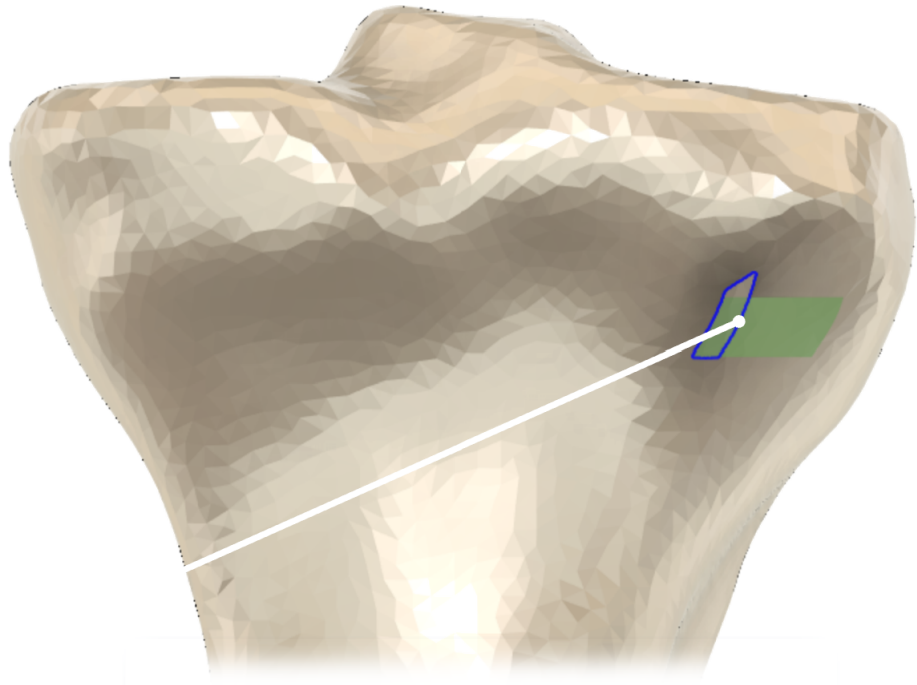


Figure 28: Both the proposed optimal apex region (blue outline) and the recommended region from literature (green region) mapped onto the surface of an average sized tibia. The osteotomy cut is shown in white, with its apex at the optimal point $w = 13$ mm, $h = 17$ mm.

An overlay of the optimal apex region found from this analysis on the average sized bone used is shown as blue outline in figure 28. The osteotomy cut is indicated, with its apex at the proposed optimal point $w = 13$ mm, $h = 17$ mm, in figure 27. The recommended range of hinge widths and heights from literature [14, 40] are shown shaded green for comparison. The proposed apex location and the majority of the optimal region lies within the recommendations from literature. The optimal region is shifted towards the upper bound on hinge width from literature due to anterior plate placement, as discussed before.

Summary: Surgical Implications

We propose an optimal apex location of $w = 13$ mm, $h = 17$ mm by combining the bounds found to prevent type III fracture in the intra-operative analysis, ensuring acceptable micromotion in the post-operative analysis, and two additional bounds from literature recommendations.

5 Investigating Plate Fixation Procedure

A fixation plate is screwed into the proximal tibia across the opened osteotomy cut during MOWHTO surgery to hold the opening in place whilst the bone heals and fills the gap. This process induces strains at the lateral hinge, which may be detrimental in the case of a fractured hinge.

The effect of altering the plate fixation procedure on strains at the lateral hinge was investigated to identify how the procedure may be improved to prevent lateral hinge fracture and further damage if a fracture has occurred. The effects of changing the order of screw insertion were explored in section 5.1 and of changing the insertion angle of the non-locking lag screw in section 5.2.

5.1 Varying Screw Insertion Order

5.1.1 Overview

The strains at the lateral hinge caused by plate fixation and the effect of changing screw insertion order were analysed through both experimental and FE methods. A two-dimensional model of the 3D tibia geometry was used in experiments and FEA for ease of analysis. Another simplification from the *in vivo* setup was the use of a truncated fixation plate to mimic holes D, 1, and 2 of the TomoFix plate (figure 12) and therefore three fixation screws instead of the eight in surgery. Through communication with Mr Melton, these were deemed to be the critical fixation points, after which there is little movement or deformation of the plate.

Results from FE methods were compared and contrasted with experimental results. The benefits of FE simulations were the speed at which they could be performed for different setups and their output of strain at any desired location. Whilst experiments were slower to conduct and only gave strain measurements at the strain gauge location (midway along the lateral hinge), they were a better representation of the interactions during surgery and results were assumed to be more comparable with reality. FE results agreed with experimental results in some cases, but disagreed in others, prompting an evaluation of the setups used for FEA. FE setups were less versatile when modelling different screwing orders and were less accurate in mimicking *in vivo* interactions.

Four different screw insertion orders were investigated as follows:

- A ‘Default’ insertion as recommended by the TomoFix manual - tighten top screw, tighten lag screw, and tighten bottom screw
- B ‘Reverse’ insertion - tighten bottom screw, tighten lag screw, and tighten top screw
- C Inspired by Mr Melton’s method - insert top screw without tightening, tighten lag screw, tighten top screw, and tighten bottom screw
- D Mr Melton’s method - insert top screw without tightening, insert lag screw without tightening, tighten top screw, tighten lag screw, and tighten bottom screw

5.1.2 Experimental Methods

Screws were inserted into the model tibia during experiments, and strains at the hinge were measured with a strain gauge. These gave an understanding of strain magnitudes and directions and the effect of changing salient variables such as torque and screw order. Torque was represented by the force applied on the end of an Allen key to tighten the screw, measured using a spring balance. Force measurement was accurate to roughly ± 2 N with the use of this equipment. Following initial experiments using a Perspex tibia, an improved model was devised to more accurately capture the plate, screw, and bone interactions that occur during surgery.

Perspex Tibia Experiments

A diagram of the initial experiment setup is shown in figure 29(a) and an image of the setup in figure 29(b). The tibia was modelled by a 12 mm thick homogeneous Perspex ‘bone’ profile taken from the same mid-thickness coronal slice used to define osteotomy cut parameters in section 4. Perspex was chosen as it models the viscoelasticity and brittle fracture of cortical bone, the region of bone in which fracture strains are critical. The bottom portion of the tibia

was replaced with an encastre (fixed) boundary condition, as this region remains a fixed rigid body during surgery.

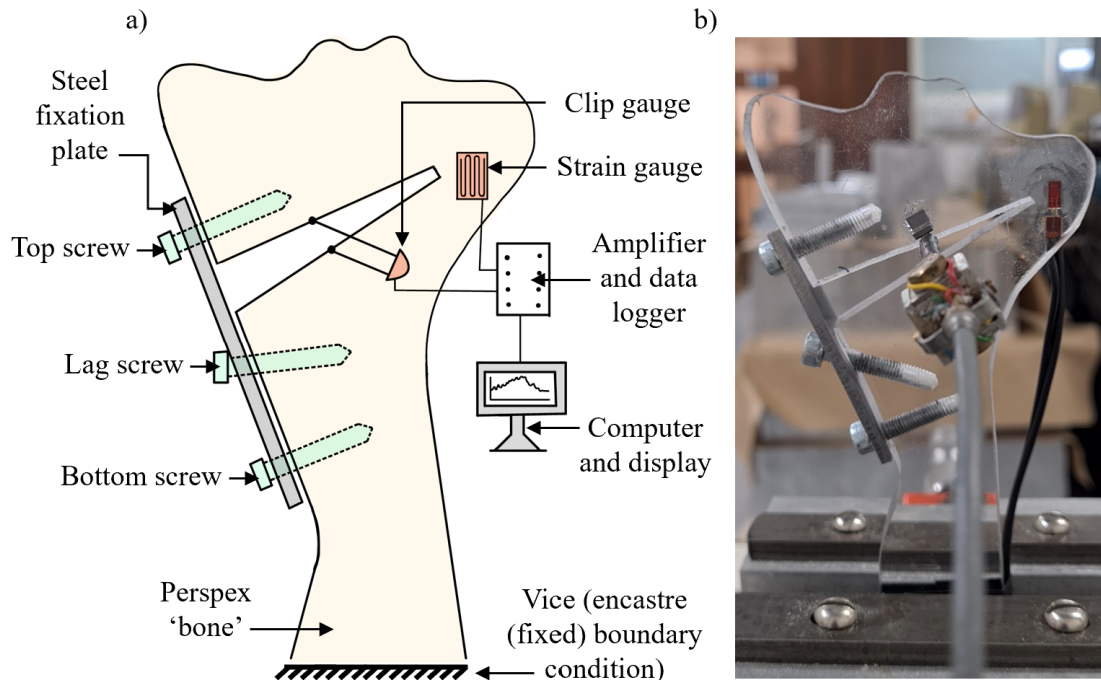


Figure 29: Initial screw experiment setup with Perspex tibia. a) Labelled diagram of equipment setup. b) Image of setup taken during an experiment in the laboratory.

The concave region of the tibia at the osteotomy cut entrance was simplified to a flat surface for ease of plate and tibia hole alignment. The titanium fixation plate was modelled by a 3 mm thick rectangular steel plate and holes for the top, lag and bottom screws were drilled in the same relative positions as holes D, 1, and 2 in the TomoFix plate, respectively (figure 31). The 5 mm diameter titanium screws used in surgery were represented by 5 mm diameter mild steel screws.

A standard 3 mm strain gauge was glued midway along the lateral hinge to measure the axial strain (along the bone's longitudinal axis) during experiments. A clip gauge was attached midway along the osteotomy cut to measure the crack opening displacement. Both of these measuring instruments were connected to a strain amplifier and data logger to log and store measurements (figure 29(a)).

The Perspex experimental model had some flaws which reduced the accuracy and repeatability of the results. The experiments had a non-repeatable nature because the Perspex underwent some plastic deformation during plate fixation. This was observed by the strain not fully returning to zero when the fixation plate and screws were removed. As the same sample was used in multiple experiments, strain magnitudes could not be compared across experiments. There was also scope for the screws to rotate relative to the plate once inserted due to the difference in screw and plate hole diameters. Model adjustments were necessary to address these issues.

Aluminium Tibia Experiments

A revised model (figure 30) was developed with input from Mr Melton, to capture the important bone, plate, and screw interactions during MOWHTO. Perspex was replaced by aluminium, as it behaves elastically up to a larger strain. This ensured strains remained within the material's elastic region so that experiments were repeatable.

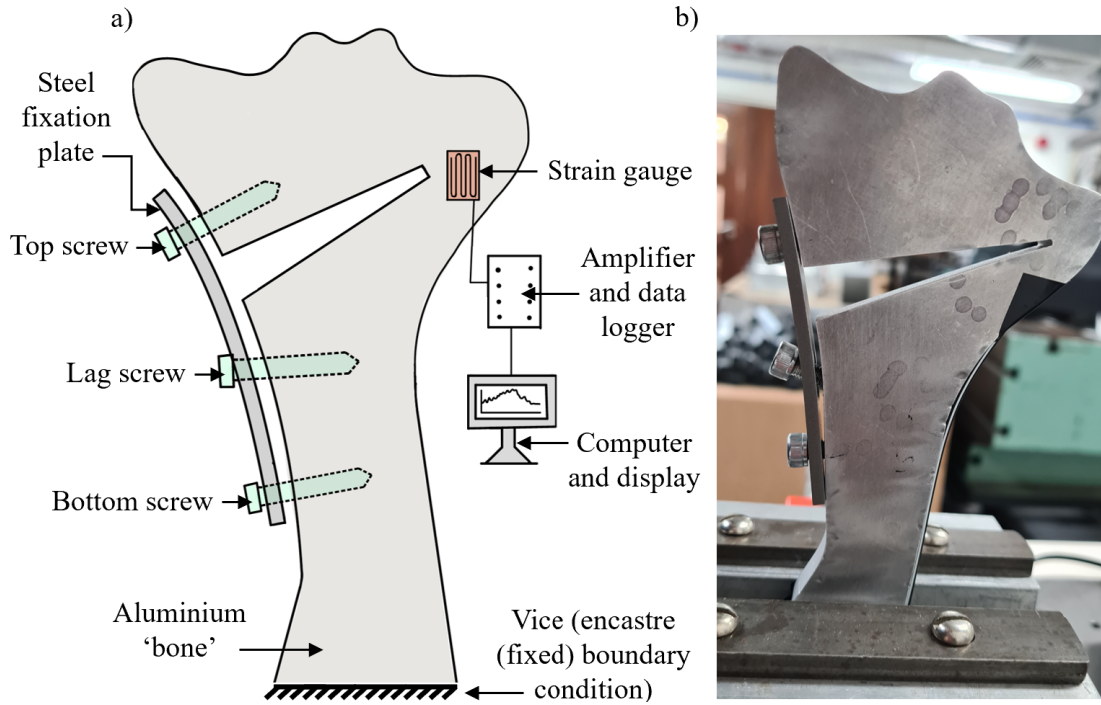


Figure 30: Revised experiment setup with metal tibia. a) Labelled diagram of equipment setup. b) Image of setup taken during an experiment in the laboratory.

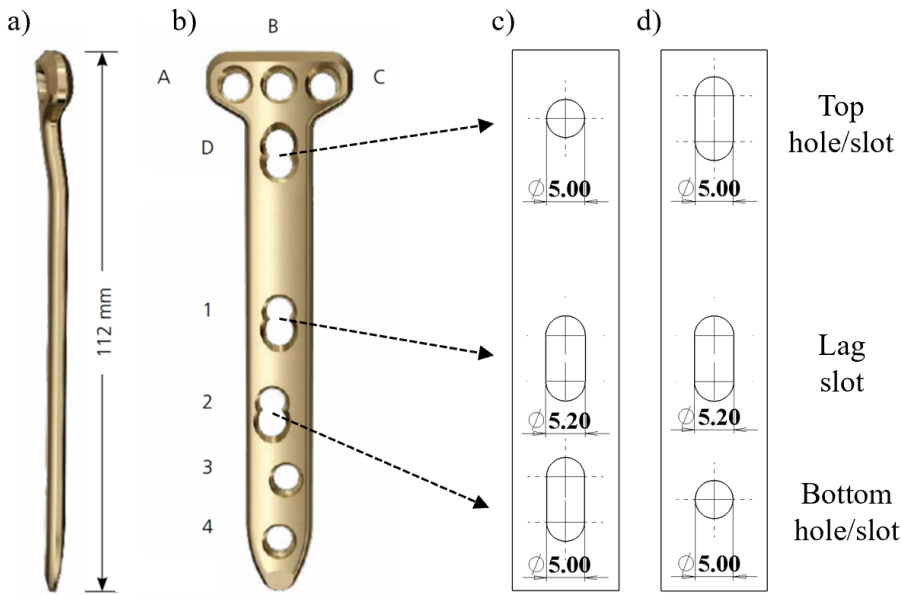


Figure 31: Comparison between TomoFix fixation plate geometry and simplified plate geometry used in this investigation. All measurements in mm. a) TomoFix plate side view [21]. b) TomoFix plate front view with labelled holes [21]. c) Simplified plate geometry for default order. d) Simplified plate geometry for reverse order.

The tibia profile around the cut entry (initially flattened) was restored to its concave curved shape, allowing the fixation plate to bend as it would *in vivo*. Slots were drilled into the steel plate to replace certain holes, allowing alignment of plate and tibia holes despite the concave profile. For order A, the lag and bottom screw holes (figure 31(c)) were replaced by slots, and for order B, the lag and top screws holes (figure 31(d)) were replaced by slots.

The contrast between the locking and non-locking screw holes modelled the different purposes of these screw types more effectively. The plate holes for locking (top and bottom) screws were reduced in diameter to 5 mm to capture the rigid body motion between the plate and 5 mm locking screws (figure 31). Rotation and translation of the screw relative to the plate was minimised. A vertical slot was drilled for the non-locking (lag) screw with a wider diameter (5.2 mm) than the locking screw holes to allow rotation of this screw relative to the plate about the y-axis.

Experiments with the improved model were more repeatable than with the initial model, as strains returned to zero whenever the fixation plate and screws were removed. The new model was assumed to produce results more representative of *in vivo* fixation, as its properties were more akin to the interactions occurring in surgery.

5.1.3 Experimental Results and Discussion

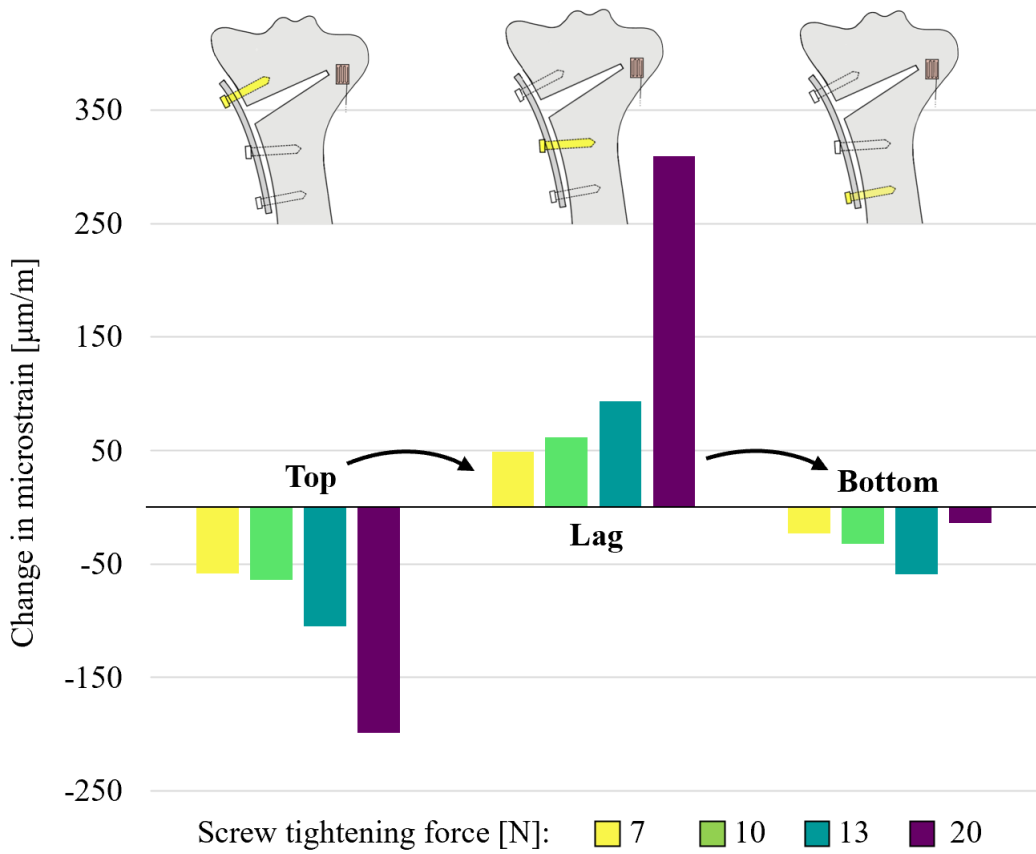


Figure 32: Vertical strains induced at the lateral hinge by the top, lag, and bottom screws, for insertion order ‘top, lag, bottom’. Four different screw tightening forces of 7, 10, 13, and 20 N were applied. Arrows indicate order of screwing.

Figure 32 shows the change in microstrain as measured by the strain gauge midway along the lateral hinge for the top, lag, and bottom screws when inserted in order A. Four different screw tightening forces were applied, indicated by different colours. The top screw induced consistently compressive strains, and the lag screw consistently tensile, with similar magnitudes. The bottom screw induced compressive strains of a smaller magnitude than other screws. Strain magnitude increased with increasing screw tightening force, except in the case of the bottom screw at 20 N. This is an anomaly likely caused by inaccurate measurement of tightening force using the spring balance, or yield in the material below the hinge which led to relaxation of the strains at the hinge.

Data from the clip gauge confirmed crack opening during compressive strains at the middle of the lateral hinge and crack closing during tensile strains.

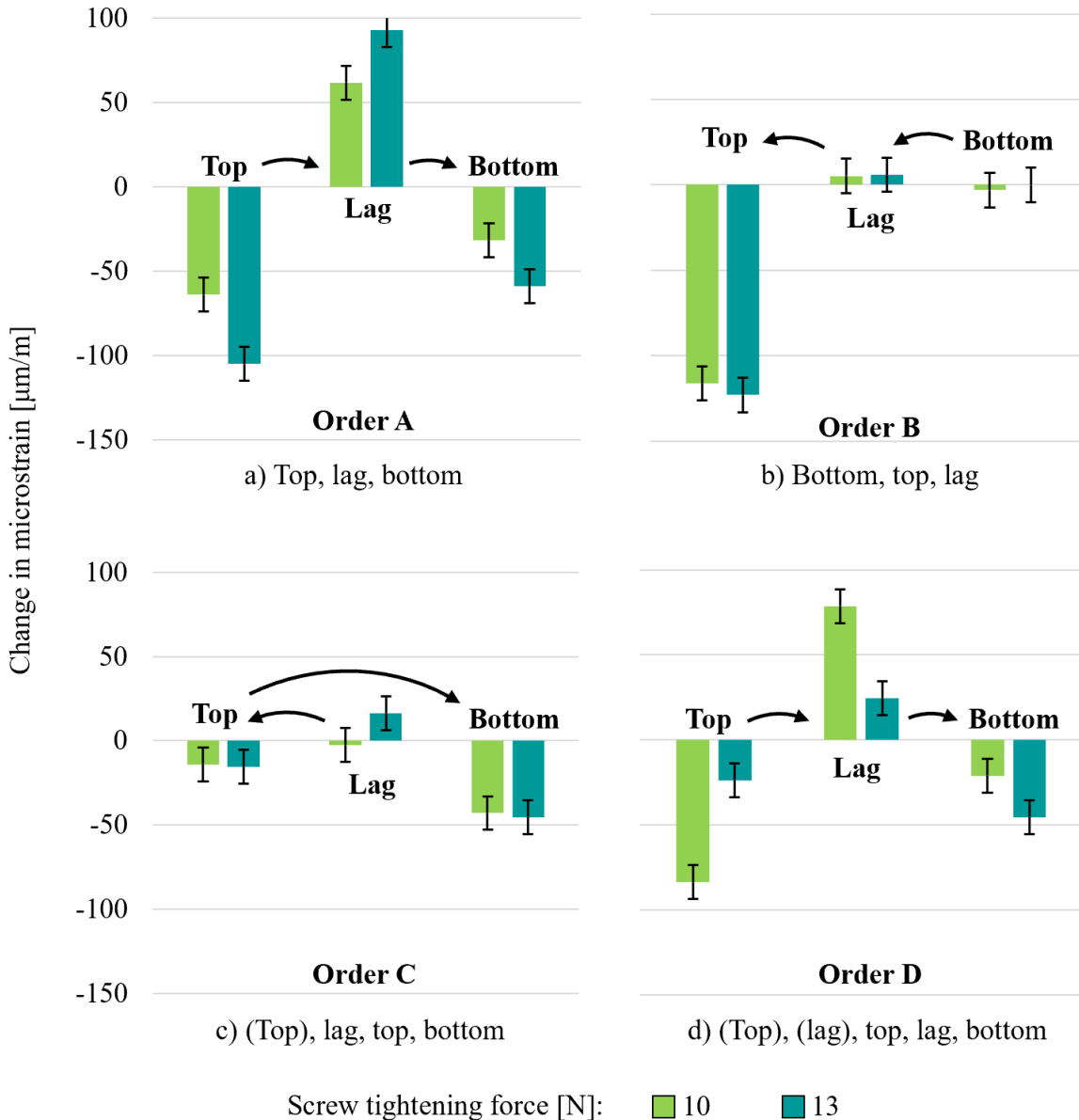


Figure 33: Vertical strains induced at the middle of the lateral hinge by the top, lag, and bottom screws, for four different insertion orders. Two different screw tightening forces of 10 and 13 N were applied. Arrows and sub figure captions indicate order of screwing; screws in brackets indicate insertion without tightening. Order B negates tensile strains. Order C minimises overall strain magnitudes and is the optimal order.

Figure 33 shows the change in microstrain midway along the lateral hinge induced by the top, lag, and bottom screws for four different insertion orders. The results for two out of four different screw tightening forces are shown for clarity, again indicated by different colours. Screw names in brackets indicate insertion of that screw without tightening, as full tightening occurs later in the sequence. Black arrows indicate order of screw tightening. Error bars of $\pm \mu\text{m}/\text{m}$ indicate fluctuation in strain measurement with no force applied.

Compared with the default sequence (order A), the reverse order (order B) induced negligible tensile strains and larger compressive strains during top screw tightening. This insertion order is

appealing to avoid tensile strains at the hinge and induce compressive strains which may enhance bone healing in the occurrence of a type I fracture. Order C, in which the top screw is first inserted but not tightened, had the smallest overall strain magnitudes. This sequence is appealing to avoid large strains in general and minimise the deformation caused by plate fixation overall. The stress-strain curves for cortical bone in section 2.2 (figure 7) show failure at lower strains in compression than tension. Order C may therefore be deemed most appropriate in preventing fracture. Strains induced by order D were not significantly different from the default sequence. It is important, however, to consider the strains along the whole length of the lateral hinge, most practical through FEA.

Summary: Screw Insertion Order Experiments

The strains midway along the lateral hinge induced by the default insertion method are compressive for the top and bottom screws, and tensile for the lag screw.

Reverse insertion may offer an improvement to the default method in the occurrence of a type I fracture, as it negates tensile strains and increases compressive strains caused by the top screw.

Insertion of the top screw without tightening, then tightening of the lag, top, then bottom screws minimises overall strain magnitudes, so may be better than the default method for preventing fracture.

5.1.4 FE Methods

Model Setup

The screw insertion process was simulated for screws of interest in separate finite element simulations. Each simulation had unique boundary conditions, whilst these were kept as consistent as possible across simulations.

A diagram of the loading and boundary conditions applied to investigate the effect of tightening the lag screw for screw orders A and B is shown in figure 34. As in the experimental configuration, the distal tibia was replaced with a fixed boundary condition and a traction force of 5 N/m was applied in opposite directions on the plate and bone hole surfaces to model tightening of this screw. The plate hole surface was pulled towards the tibia and the tibia hole surface was pulled towards the plate. The traction force was chosen empirically such that movement and bending of the plate was small.

To mimic screwing order A, a coupling constraint was applied between the top tibia and plate hole surfaces to model a locking screw holding these parts together rigidly (figure 34(a)). Similarly, for screwing order B, a coupling constraint was applied between the bottom tibia and plate hole surfaces (figure 34(b)). Fixing of the plate with an encastre boundary condition was necessary to allow the simulation to run, so the top face of the plate was chosen for fixing in both cases for consistency.

Figure 35 shows the loading and boundary conditions applied to investigate the effect of tightening the top screw for screw orders A and B. The setup is similar to that of the lag screw. There was no coupling constraint for order A (figure 35(a)), since the top screw is the first inserted, but the top of the plate was fixed in place to allow the simulation to run. For order B (figure 35(a)), as well as a coupling constraint between bottom hole surfaces, a coupling constraint with allowed

rotation was applied between lag hole surfaces. This permitted the plate to rotate relative to the tibia, modelling the ability of the lag screw to rotate and the plate to bend *in vivo*.

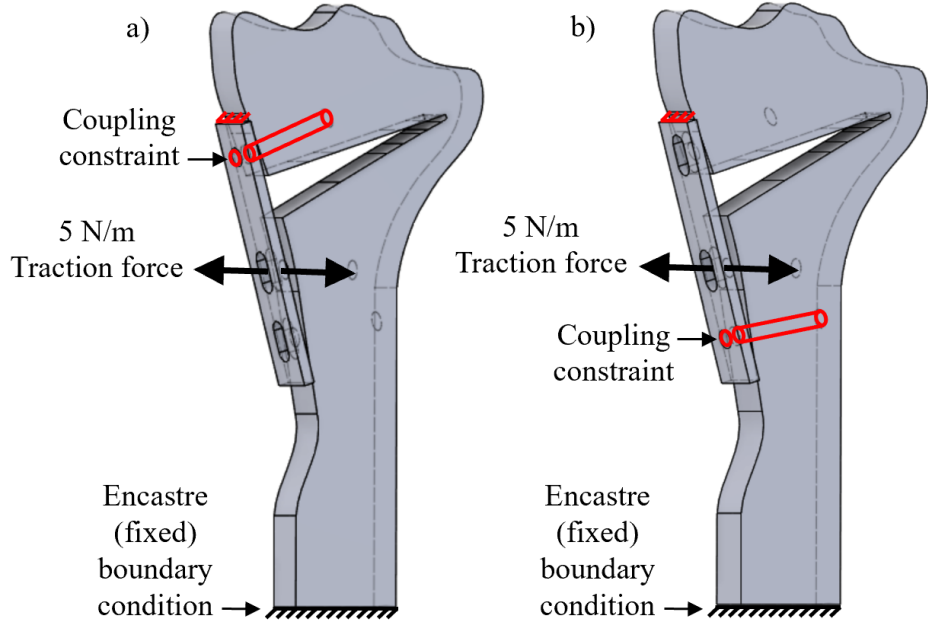


Figure 34: Simplified model setup to investigate strains induced by the lag screw for screwing orders a) top, lag, bottom, and b) bottom, lag, top. Boundary conditions and constraints are labelled. Coupling constraints in red signify no translation or rotation between plate and tibia screw holes.

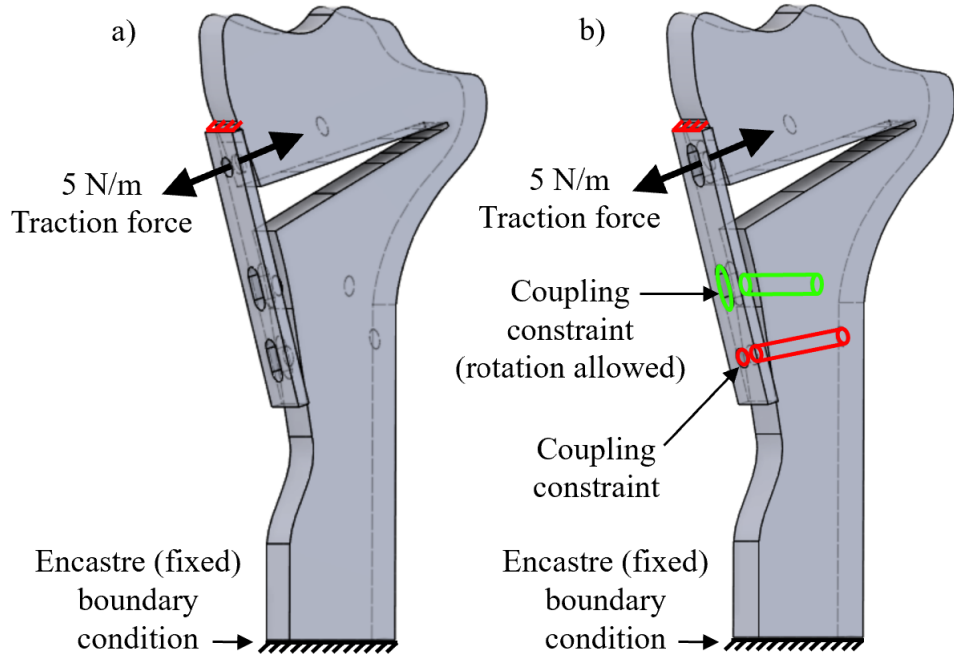


Figure 35: Simplified model setup to investigate strains induced by the top screw for screwing orders a) top, lag, bottom, and b) bottom, lag, top. Boundary conditions and constraints are labelled. Coupling constraints in red signify no translation or rotation between plate and tibia screw holes. Coupling constraints in green signify no translation between the plate and tibia screw holes, allowing rotation between them.

The FE mesh was refined in the vicinity of the apex and along the lateral hinge, and the surface path along which strain were plotted is shown in figure 36.

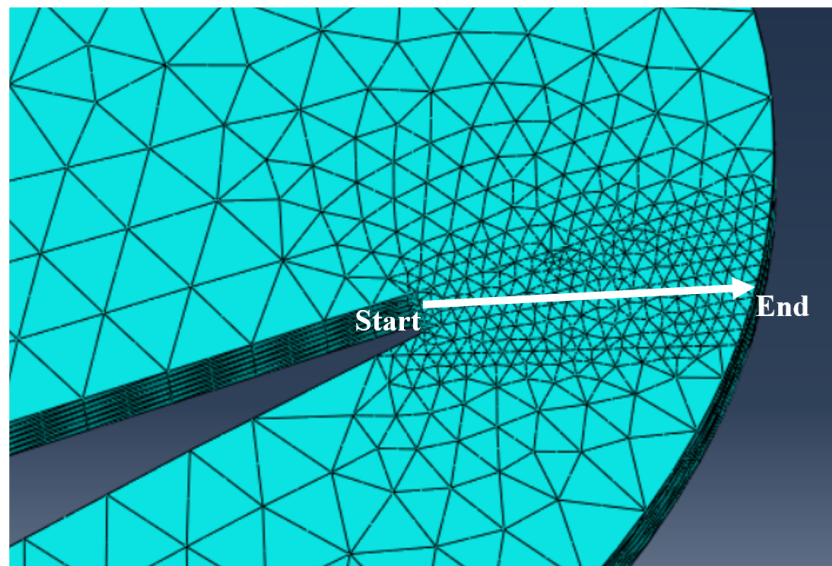


Figure 36: Mesh refinement at the lateral hinge and line (in white) along which strains were measured and plotted.

5.1.5 FE Results and Discussion

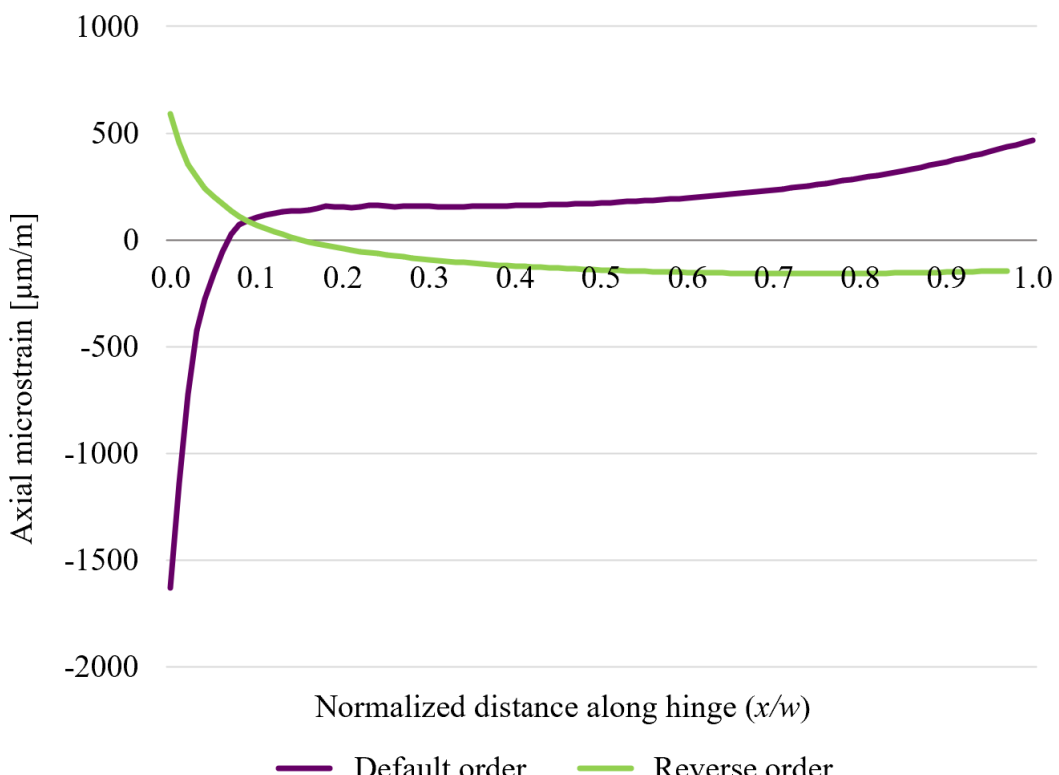


Figure 37: Strains predicted by FEA along the lateral hinge induced by the lag screw for the default and reverse screwing orders.

The microstrain along the lateral hinge when inserting the lag screw for screwing orders A and B is shown in figure 37. For order A, strains are tensile throughout the hinge, except across the first 10% of the hinge closest to the apex. This agrees with the tensile strains from experiments found at $x/w = 0.5$ for the lag screw. For order B, strains are in the opposite direction and have smaller magnitude; the majority of the hinge is under compression, favourable in the event of a type I fracture. The concept of minimising tensile stresses using order B matches experimental results, when the extension of the error bar into the compressive region for the lag screw (figure 33) is considered.

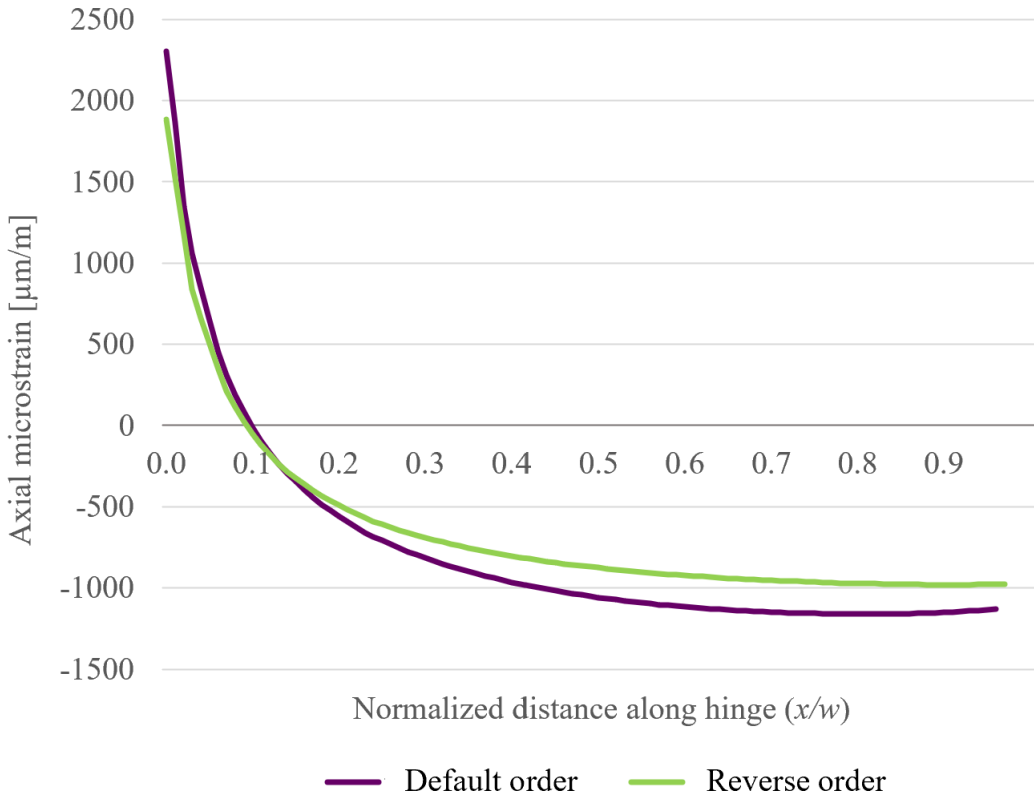


Figure 38: Strains predicted by FEA along the lateral hinge induced by the top screw for the default and reverse screwing orders.

Figure 38 shows the microstrain along the lateral hinge when inserting the top screw for screwing orders A (default method) and B (reverse method). The tensile strain is on average 20% smaller and the compressive strain 15% smaller for order B compared with order A. Although both orders give compression at $x/w = 0.5$ matching experiment strain directions, this contrasts the stronger compression seen for order B in experiments and questions the validity of the setup used in figure 35. The smaller strains may be a result of the encastre boundary condition applied at the top of the plate, a constraint that is not present as such during surgery.

The contrast between some FE results and experimental results suggests that a revision of the FE setups used is needed before FE results can produce meaningful conclusions. This is expanded upon in section 6

The FEA shows strains across the whole length of the lateral hinge, providing greater insight into experimental results. Figures 37 and 38 show that the highest strain magnitude is at the apex, and that strains switch direction at around $x/w = 0.1$. In experiments, the reverse screwing order induced more compression at $x/w = 0.5$, suggesting large tensile strains at the apex.

Partial insertion of the top screw before the lag screw minimised both tensile and compressive strain magnitudes at $x/w = 0.5$, suggesting smaller strains at the apex, the critical location for fracture prevention. This corroborates the merits of using the partial insertion method, or order C.

Summary: Screw Insertion Order FEA

The FE model and boundary constraints used to investigate lag screw insertion in the default insertion order gives results that agree with experiments. The reverse screw order works to minimise tensile strains caused by the lag screw.

FE models were a less accurate representation of the interactions during surgery than experiment models. They thus require revision to better mimic surgical mechanics, as some results deviate from experimental results. comparable with reality.

5.2 Varying Lag Screw Angle

5.2.1 Methods

The effect of varying the insertion angle of the lag screw on strains at the lateral hinge was investigated using FEA. The geometry was kept more consistent between different lag screw angle simulations as a result. Experiments would have required multiple different tibia models which were likely to vary slightly in shape due to machining tolerances and the angle of the lag screw tibia hole would have had a poor accuracy of $\pm 5^\circ$. Provisional perspex experiments were carried out comparing two different lag screw angles, but strain magnitudes were not comparable due to slight variation in the strain gauge placement between models. FE methods allowed the points of strain measurement to be identical between models.

The setup used was the same as that used to investigate the lag screw for screw order A, shown in figure 34(a), because this setup matched experimental results and was hypothesized to mimic *in vivo* interactions the most accurately (section 5.1.4). A coupling constraint was applied between the top tibia and plate hole surfaces to model a locking screw holding these parts together rigidly, and 5 N/m traction was applied between the lag hole surfaces to mimic lag screw tightening. The angle of the lag screw was altered between simulations, but all other model aspects remained the same.

5.2.2 Results and Discussion

Three different lag screw angles were investigated: a horizontal screw at 0° , a 10° distal rotation, and a 20° distal rotation. The strain across the hinge for these screw angles is shown in figure 39. Mr Melton hypothesized that aiming the lag screw distally would reduce tensile strains at the lateral hinge.

The most significant points of difference between the varying lag screw angles are highlighted in figure 39. In the vicinity of the apex, 10 - 20% of the way along the lateral hinge, aiming the lag screw distally reduced the local maximum tensile strain by 50%, a significant reduction, in agreement with Mr Melton's hypothesis. There is negligible different between the strain for both the distal rotations here. Near the lateral cortex ($x/w \approx 1$) is the next most significant point of difference between the three lag angles. Strain for the 10° and 20° distal screws are 8% and 14% smaller than the horizontal screw, respectively.

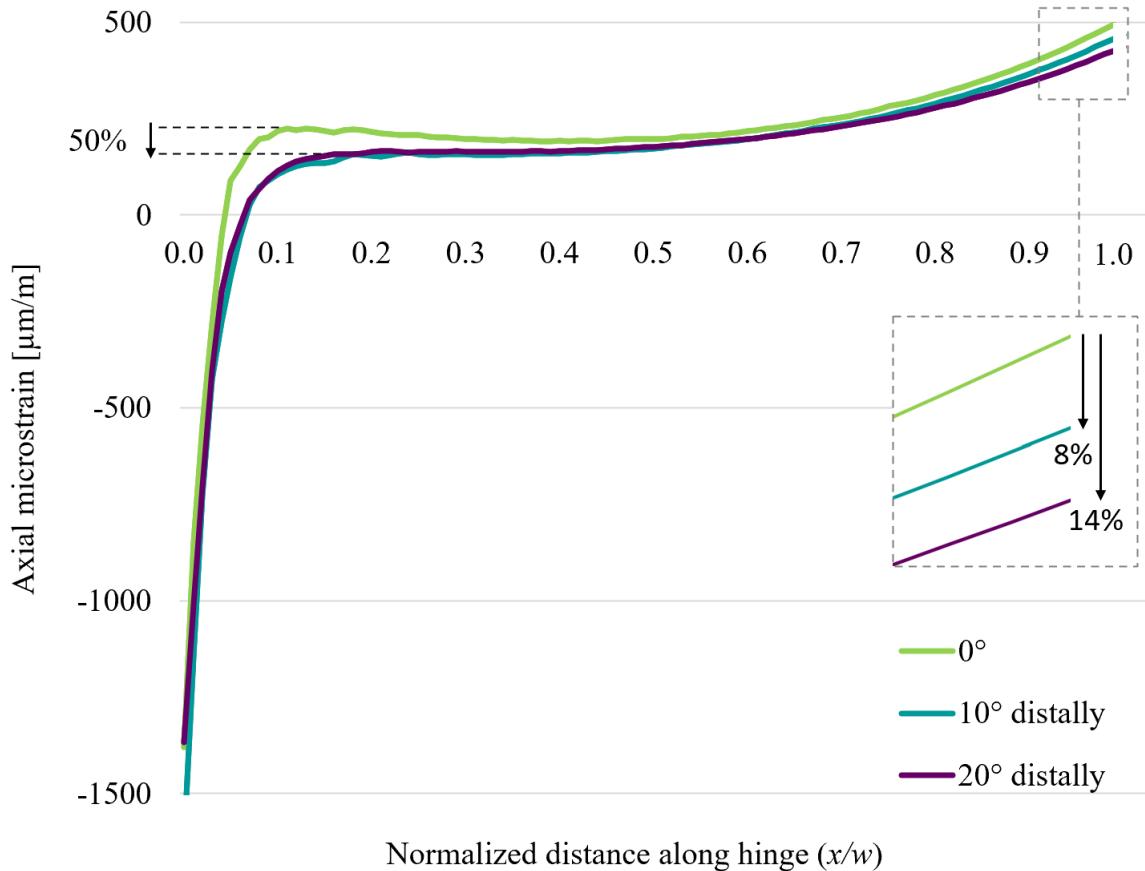


Figure 39: Strains predicted by FEA along the lateral hinge induced by the lag screw for three different lag screw insertion angles relative to the horizontal axis. Default screwing order used in all cases.

Summary: Lag Angle FEA

Aiming the lag screw 10° or 20° distally reduces maximum tensile strains near the apex by 50%, agreeing with Mr Melton's hypothesis.

6 Limitations and Further Research

This work thoroughly examined the optimal apex position on a single *model knee*. It would be beneficial to obtain the optimal apex position to minimise surgical risk for any bone from its geometry. Analysis on the optimal osteotomy apex position in section 4 could be extended to other tibia geometries to investigate the variation of the optimal region with various tibia parameters. A similar analysis was conducted by Earl (2021) [6], but would benefit from using the same cortical and trabecular 3D geometry as in this analysis, and a more extensive variation of apex locations.

In order to limit the number of apex locations for which to run a full FE simulation, a Bayesian optimization algorithm could be used to determine the next apex location point to acquire for a new bone geometry to maximise information gain. The bounds found in this investigation could be input into the algorithm as a prior. The algorithm would determine which (w, h) to simulate next, to obtain information about the bound for a different tibia most efficiently. This step would be repeated until the computer reaches a confidence threshold for the bound in question. The

result would be an estimate of the optimal apex region for a set of varying tibia geometries, avoiding running expensive FE simulations at many (w , h) combinations.

Another useful study may help further justify the strain nucleation fracture classification method used in this analysis and determined experimentally by Tomaszczyk (2020) [13]. Fracture of the tibia could be simulated with finite element models for various lateral hinge geometries, and the location of the fracture nucleation point observed. This analysis would benefit from modelling the material and mechanical properties of bone as accurately as possible by including plasticity and failure strain, although simulations would have long run-times.

The effect of plate placement on construct stability could also be investigated to help provide more detailed guidance to surgeons when positioning the plate. For example, weight-bearing for medial versus anterior placement could be simulated and micromotion quantified and compared. If stability is sensitive to plate position, then different optimal apex regions could be proposed depending on the planned plate placement.

Further experimental work could be conducted using digital image correlation to quantify the strains along the whole lateral hinge during screw insertion to see how these compare to FE results. 3D bone models such as Sawbones [46] could also be used in experiments to see whether the 2D results are consistent with results using 3D models. Different FE models to investigate screw insertion could be explored to determine the method which best represents *in vivo* interactions. This may involve developing a crude 3D simplification of the bone geometry, plate, and screws and simulating friction between these.

7 Conclusions

One of the most common complications in MOWHTO surgery is lateral hinge fracture. A literature review and guidance by Mr Melton identified the location of the lateral hinge and the procedure of plate fixation as salient factors affecting fracture likelihood and surgical success. The project aims were formulated as 1: finding the optimal apex location for minimising the expected surgical risk, considering intra-operative fracture likelihood and severity, and post-operative stability, using a 3D model with two bone material regions and 2: finding the strains at the lateral hinge during plate fixation and how adaptations to the procedure may affect these.

Results from this study concerned with the first aim of recommending an optimal apex location supported the trends seen in literature regarding the effect of the cut apex position on the likelihood and type of fracture. Both wider hinges and those closer to the tibial plateau were shown to increase type III fracture risk. Wide hinges were shown to reduce micromotion of the cut, increasing stability. Results have also suggested that there is likely an apex region which minimises the expected surgical risk. Intra-operative simulations gave an apex locus bound for an average sized tibia to prevent type III fracture during the osteotomy cut opening. Post-operative simulations gave two more bounds to ensure micromotion of the cut lay within an acceptable range.

Bounds from intra-operative and post-operative analyses, as well as relevant literature were combined to give the proposed optimal apex position as $w = 13$ mm, $h = 17$ mm. This point lies within the range of lateral hinge widths and heights employed in surgery and quoted in literature, and contributes to the literature by recommending a specific point rather than the fairly loose bounds available priorly. Whilst the proposed hinge height in this analysis was very similar to an average height calculated from values given across studies, the hinge width was greater than the average width. This was likely caused by the anterior fixation plate placement, which favoured

wider hinges to prevent excessive micromotion than other recommendations.

Results from screw insertion experiments demonstrated that during the default insertion order, the top screw compresses the lateral hinge, the lag screw imposes tensile strains on the hinge, and the bottom screw imposes small compressive strains on the hinge. The reverse order imposed negligible tensile strains, and slightly more compressive strain at the lateral hinge, and this method may be beneficial in the case of a type I fracture. Inserting the top screw without tightening, then tightening in the order lag, top, and bottom minimised strain magnitudes across all screws. This method, partly inspired by Mr Melton's proposed insertion method, was judged to be the best of the screw insertion methods investigated for preventing fracture, as cortical bone stress-strain curves revealed large compression magnitudes to be more severe than small tensile strains. The latter two methods are worth further investigation with 3D physical and FE models, to confirm whether these conclusions translate to the 3D case.

FEA on different screw insertion orders revealed that the model used should be adjusted in certain cases to represent the *in vivo* interactions more accurately. The setup used to model lag screw tightening gave strains which matched experimental results, and hence, this model was used in the lag screw angle investigation. Tightening the bottom screw before the lag screw helped to negate the tensile strains caused by the lag screw, in agreement with the experiments. Results for top screw tightening, however, contrasted with experimental results; this model is in need of revision. Investigation of the effect of varying the lag screw angle using FEA revealed that aiming the lag screw distally by 10° and 20° reduced the tensile strains at the lateral hinge by 50%, in alignment with the hypothesis.

In summary, the main contributions of this work to research in knee stabilisation surgery are the proposal of an optimal cut apex position and an alternative plate fixation method to minimise surgical risk in MOWHTO surgery.

8 Acknowledgements

I would like to extend my sincere thanks to Professor Michael Sutcliffe of the Engineering Department, University of Cambridge, for his supervision during this research project, as well as Mr Joel Melton of Cambridge University Hospitals NHS Trust for his guidance.

I would further like to thank Dr Neil Segal of the University of Kansas Medical Center and Dr Tom Turmezei of Norfolk and Norwich University Hospitals NHS Foundation Trust for the provision and review of the patient CT data that was used throughout this project. Many thanks, also, to Rosemary Earl and Stanisław Tomaszczyk for their former work in this field, which I had the pleasure of building upon. Extended thanks to Rosemary for the additional advice she provided.

References

- [1] Public Health England. Prevalence of osteoarthritis in England and local authorities: Birmingham. <https://www.versusarthritis.org/media/13374/birmingham-oa-1.pdf> (accessed 24/05/2022), 2013.
- [2] N. Domenico. Bilateral proximal tibial stress fractures, Patient data - age: 55 years, gender: Male. <https://radiopaedia.org/cases/bilateral-proximal-tibial-stress-fractures> (accessed 25/05/2022).

- [3] P. Niemeyer et al. Two-year results of open-wedge high tibial osteotomy with fixation by medial plate fixator for medial compartment arthritis with varus malalignment of the knee. *Arthroscopy : The Journal of Arthroscopic & Related Surgery : official publication of the Arthroscopy Association of North America and the International Arthroscopy Association*, 24 7:796–804, 2008.
- [4] R. Takeuchi et al. A new classification of lateral hinge fracture. *Arthroscopy: The Journal of Arthroscopic & Related Surgery*, 2012.
- [5] K. T. Kang et al. Biomechanical effect of a lateral hinge fracture. *Journal of Orthopaedic Surgery and Research*, 2020.
- [6] R. Earl. Preventing Lateral Hinge Fracture in High Tibial Osteotomy. *MEng Report, University of Cambridge*, 2021.
- [7] A. Boström et al. Hinge location and apical drill holes in opening wedge high tibial osteotomy: A finite element analysis. *Journal of Orthopaedic Research®*, 39:628 – 636, 2020.
- [8] Boroondara Osteopathy. Knock Knees? <https://boroondaraosteopathy.com.au/knockknees/> (accessed 01/06/2022), 2019.
- [9] M. F. Schubert et al. Failures of Realignment Osteotomy. *Operative Techniques in Sports Medicine*, 28:150714, 2020.
- [10] X. Liu others. High Tibial Osteotomy: Review of Techniques and Biomechanics. *Journal of Healthcare Engineering*, 2019, 2019.
- [11] B. Ollivier et al. Good long-term survival and patient-reported outcomes after high tibial osteotomy for medial compartment osteoarthritis. *Knee Surgery, Sports Traumatology, Arthroscopy*, 29:3569 – 3584, 2020.
- [12] I. El-Ganzoury et al. Unicompartmental knee arthroplasty versus high tibial osteotomy in treatment of isolated medial compartment osteoarthritis of knee: A Systematic Review and Metaanalysis. *QJM: An International Journal of Medicine*, 2021.
- [13] S. Tomaszczyk. Lateral hinge fracture in high tibial osteotomy. *MEng Report, University of Cambridge*, 2020.
- [14] R. Nakamura et al. Appropriate hinge position for prevention of unstable lateral hinge fracture in open wedge high tibial osteotomy. *The Bone & Joint Journal*, 99B:1313–1318, 2017.
- [15] R. M. A. Raja Izaham et al. Finite element analysis of Puddu and Tomofix plate fixation for open wedge high tibial osteotomy. *Injury*, 43 6:898–902, 2012.
- [16] J. Dexel et al. Open-wedge high tibial osteotomy: incidence of lateral cortex fractures and influence of fixation device on osteotomy healing. *Knee Surgery, Sports Traumatology, Arthroscopy*, 25:832–837, 2015.
- [17] H. Peng et al. Osteotomy Around the Knee: The Surgical Treatment of Osteoarthritis. *Orthopaedic Surgery*, 13:1465 – 1473, 2021.

- [18] S.Kim et al. Biplanar Medial Open-wedge High Tibial Osteotomy for Medial Compartment Osteoarthritis of the Knee: A Novel Technique and Follow-up. *Operative Techniques in Orthopaedics*, 17:29–37, 2007.
- [19] K. W. Nha et al. Uniplane medial opening wedge high tibial osteotomy relative to a biplane osteotomy can reduce the incidence of lateral-hinge fracture. *Knee Surgery, Sports Traumatology, Arthroscopy*, 28:1436–1444, 2019.
- [20] J. Oliver. Anatomical planes. <https://teachmeanatomy.info/the-basics/anatomical-terminology/planes/> (accessed 23/05/2022), 2018.
- [21] DePuySynthes. Tomofix™ Medial High Tibial Plate (MHT), Surgical Technique. <http://synthes.vo.llnwd.net> (accessed 01/06/2022), 2017.
- [22] Physiopedia. Weight bearing. <https://www.physio-pedia.com> (accessed 18/05/2022).
- [23] S. Sabzevari et al. High Tibial Osteotomy: A Systematic Review and Current Concept. *The Archives of Bone and Joint Surgery*, 4 3:204–12, 2016.
- [24] J. A. Gasser and M. Kneissel. Bone Physiology and Biology. *BoneKEy Reports*, 2017.
- [25] Laboratoires Servier. Spongy bone - Trabecular bone - Normal trabecular bone. https://commons.wikimedia.org/wiki/File:Spongy_bone_-_Trabecular_bone_-_Smart-Servier.jpg (accessed 01/06/2022), 2019.
- [26] C. Brown et al. Time-Dependent Circumferential Deformation of Cortical Bone Upon Internal Radial Loading. *Journal of Biomechanical Engineering*, 124:456–61, 09 2002.
- [27] N. H. Hart et al. Mechanical basis of bone strength: influence of bone material, bone structure and muscle action. *Journal of Musculoskeletal & Neuronal Interactions*, 17:114 – 139, 2017.
- [28] OrthoBullets. Types of bone. <https://www.orthobullets.com/basic-science/9001/types-of-bone> (accessed 29/05/2022), 2021.
- [29] P. Augat and S. Schorlemmer. The role of cortical bone and its microstructure in bone strength. *Age and Ageing*, 35 Suppl 2:ii27–ii31, 2006.
- [30] U. Wolfram and J. J. Schwiedrzik. Post-yield and failure properties of cortical bone. *BoneKEy Reports*, 5:829, 2016.
- [31] E. F. Morgan et al. The Bone Organ System. *Osteoporosis*, 2008.
- [32] R. O. Ritchie et al. A fracture mechanics and mechanistic approach to the failure of cortical bone. *Fatigue & Fracture of Engineering Materials & Structures*, 28:345–371, 2005.
- [33] K. Piekarski. Fracture of Bone. *Journal of Applied Physics*, 41:215–223, 1970.
- [34] R. K. Nalla et al. Fracture in human cortical bone: local fracture criteria and toughening mechanisms. *Journal of Biomechanics*, 38 7:1517–25, 2005.
- [35] P. Ziopoulos et al. Microcracking damage and the fracture process in relation to strain rate in human cortical bone tensile failure. *Journal of Biomechanics*, 41 14:2932–9, 2008.

- [36] B. S. Miller et al. Complications after medial opening wedge high tibial osteotomy. *Arthroscopy : The Journal of Arthroscopic & Related Surgery : official publication of the Arthroscopy Association of North America and the International Arthroscopy Association*, 25:639–46, 2009.
- [37] R. Nakamura et al. The validity of the classification for lateral hinge fractures in open wedge high tibial osteotomy. *The Bone & Joint Journal*, 97-B:9:1226–31, 2015.
- [38] P. Chen et al. Biomechanical evaluation of different types of lateral hinge fractures in medial opening wedge high tibial osteotomy. *Clinical Biomechanics*, 83:105295, 2021.
- [39] TeachMe Surgery. Tibial Plateau Fracture. <https://teachmesurgery.com/orthopaedic/knee/tibial-plateau-fracture/> (accessed 31/05/2022), 2021.
- [40] H. Ogawa et al. The prevention of a lateral hinge fracture as a complication of a medial opening wedge high tibial osteotomy: A case control study. *The Bone & Joint Journal*, 99B:887–893, 2017.
- [41] S. Han et al. A “safe zone” in medial open-wedge high tibia osteotomy to prevent lateral cortex fracture. *Knee Surgery, Sports Traumatology, Arthroscopy*, 21:90–95, 2011.
- [42] Y. Koh et al. Multi-objective design optimization of high tibial osteotomy for improvement of biomechanical effect by using finite element analysis. *Journal of Orthopaedic Research®*, 36, 2018.
- [43] H. Kyung et al. Biplanar Open Wedge High Tibial Osteotomy in the Medial Compartment Osteoarthritis of the Knee joint: Comparison between the Aescula and Tomofix Plate. *Clinics in Orthopedic Surgery*, 7:185 – 190, 2015.
- [44] Orthopaedic Trauma. High Tibia Valgisation Osteotomy HTO Open Wedge with the Tomofix System. <https://www.youtube.com/watch?v=8MMKZehhvQ> (accessed 30/05/2022).
- [45] A. D. Kaze et al. Mechanical strength assessment of a drilled hole in the contralateral cortex. *Journal of experimental orthopaedics*, 2017.
- [46] Sawbones. Biomechanical Materials for Precise, Repeatable Testing. <https://www.sawbones.com/biomechanical-product-info> (accessed 20/05/2022), 2017.
- [47] J. C. Yang et al. Biomechanical evaluation of high tibial osteotomy plate with internal support block using finite element analysis. *PLoS ONE*, 16, 2021.
- [48] Y. Lu. Computational modelling of bone microstructure. *Computational Modelling of Biomechanics and Biotribology in the Musculoskeletal System (Second Edition)*, Woodhead Publishing, pages 251–276.
- [49] C. Luo et al. Placement-induced effects on high tibial osteotomized construct - biomechanical tests and finite-element analyses. *BMC Musculoskeletal Disorders*, 16, 2015.

Appendix A

Table 2: Maximum von Mises stresses (GPa) for intra-operative simulations with different lateral hinge widths w , and heights h .

h [mm]	w [mm]												
	4	5	6	7	8	9	10	12	14	16	17	18	20
7	1.79	1.95	2.16	-	-	-	-	-	-	-	-	-	-
8	-	-	2.32	2.31	2.35		2.63	3.85	-	4.38	-	-	-
9	-	-	-	-	2.28	2.23	2.47	2.82	4.67	-	-	-	-
10	-	-	-	-	2.22	-	2.51	2.88	3.22	5.06	5.22	5.17	-
11	-	-	-	-	-	-	-	-	-	-	4.74	5.84	6.10
12	-	-	-	-	2.40	-	2.90	3.14	3.23	4.16	-	4.90	-

Table 3: Type I to type III transition points in (w, h) using the apex corner strain nucleation fracture classification method. Apex locations (w, h) which were not simulated are indicated by '-'.

w [mm]	4	7	9	16	18
h [mm]	7	8	9	10	11

Table 4: Type I to type III transition points in (w, h) using the wider strain distribution fracture classification method.

w [mm]	4	7	9	12
h [mm]	7	8	10	12

Appendix B

Risk Assessment Retrospective

A hazard assessment was conducted at the start of the project which identified certain lab equipment and long periods of computer usage as risks to health and safety. The assessment reflected the actual hazards encountered well, and overestimated risk in places.

The use of hazardous workshop equipment such as drills and saws was carried out by trained members of staff. Measures were taken against hazards posed by electrical equipment and sharp Perspex corners when conducting screw insertion experiments. Appropriate measures were also taken to moderate screen use during finite element modelling and report writing. Overall, risks were identified and managed well, and not much change would be made to the process in retrospect.

Appendix C

The University of Kansas Medical Center

Human Research Protection Program

APPROVAL OF SUBMISSION

January 7, 2021

Neil Segal
nsegal@kumc.edu

Dear Neil Segal:

On 1/7/2021, the IRB approved the following submission:

Type of Review:	Flexible IRB Review
Reviewed by:	KUMC Human Research Protection Program
IRB#:	STUDY00146751
Title:	Determining optimum cut geometry for a medial opening wedge high tibial osteotomy (MOWHTO) to minimize risk of lateral hinge fracture
Investigator:	Neil Segal
Funding:	None
Documents submitted for the above review:	• ProtocolAndApplicationForSecon_2020-12-22_1111.pdf
Special Determinations:	None

This project was reviewed and approved under the KUMC Policy for Flexible IRB Review. It is eligible for Flexible IRB Review because it is minimal risk and is not associated with any federal funding or support. As such, you are under this KUMC policy, rather than federal regulations, when you conduct the research.

This review and approval is granted because you attested that it meets the criteria for Flexible IRB Review. If there is a change to any of the conditions listed below, you must promptly notify the IRB office so that the project can be re-reviewed under the federal regulations governing human subjects research.

Research eligible for Flexible IRB Review meets all the following characteristics:

- Not funded by a direct federal grant
- Not funded through a sub-award or pilot grant associated with federal dollars
- Does not include personnel on a federally-funded training grant
- Is not research conducted under a no-cost extension

- No data will be used to support a pending application for FDA approval or a grant application (e.g., data collection in response to a scored grant submission with plans to re-submit)
- Does not involve an FDA-regulated product or dietary supplement
- Does not involve registries about FDA-regulated products
- Is not conducted under a contract that requires the investigator to adhere to federal human subjects regulations (e.g., 45 CFR 46, 34 CFR 97 or other references to the HHS Common Rule)
- Does not involve any services that could be billed to a federal program

Your approved documents for this study are stored in the “Documents” tab in the eCompliance system.

If you have any questions regarding the human subject protection process, please do not hesitate to contact our office at 913-588-1240 or IRBhelp@kumc.edu.

Sincerely,

Karen Blackwell

List of Figures

1	Labelled surgical CT scan, based on [2, 3]. a) Before MOWHTO surgery. b) After MOWHTO surgery.	1
2	Diagram of human knee anatomy, based on [8, 9] a) Legs with an ideal mechanical axis. b) Legs with the varus deformity. c) The knee joint.	4
3	Medical Opening Wedge High Tibial Osteotomy (MOWHTO) surgical sequence. a) The osteotomy cut is made. Initially, the medial compartment carries most of the patient's weight, indicated by the long red arrow. b) The cut is opened up using a bone spreader. c) A fixation plate is screwed in to support the bone as it heals. After surgery, the patient's weight is carried more evenly across both medial and lateral compartments, indicated by the balanced green arrows.	5
4	Tibiofemoral joint anatomy and definitions, based on [2].	6
5	Coronal, sagittal, and transverse plane definition [20].	7
6	Bone structure, based on [24, 25, 26].	8
7	Stress-strain curves for cortical and trabecular bone in tension and compression [31].	9
8	Toughening mechanisms in cortical bone, based on [32]. a) Crack deflection. b) Collagen fibre bridging. c) Uncracked ligament bridging. d) Microcracking.	10
9	Quantification of osteotomy cut micromotion after MOWHTO, based on [5].	11
10	Takeuchi fracture classifications [9]	11
11	Summary of apex location recommendations from literature, based on [2].	12
12	Osteotomy fixation with the TomoFix plate, based on [21]. a) TomoFix hole names for reference. b) Proximal plate fixation. c) Distal plate fixation.	13
13	Project structure, * indicates deliverables.	15
14	Osteotomy cut parameters. w : width of the lateral hinge, h : vertical distance from apex to tibial plateau, and h_0 : vertical distance from cut entry to tibial plateau.	16
15	2D coronal plane tibia profile extracted at mid-thickness to define cut parameters w and h	17
16	Section views of proximal tibia meshes derived from patient CT scan. a) Original dense mesh, solely consisting of cortical bone. b) Decimated mesh, consisting of cortical shell and trabecular inner solid.	19
17	Intra-operative model labelled with boundary conditions and constraints. Upwards displacement applied at the cut entrance to mimic cut opening, and nodes in the vicinity of applied displacement point constrained to move as a rigid body.	20
18	Local mesh seed settings at apex region (in mm); global seed spacing is 5 mm. a) Reference mesh with large apex refinement. b) Mesh used in intra-operative simulations. Diagram not to scale.	20
19	Fracture classification by location of strain nucleation, based on results by Tomaszczyk [13]. The region of bone shown is the lateral tibia shoulder. Type I fractures nucleate at the lower apex corner and type III at the upper apex corner.	21
20	Stresses at the apex after cut opening simulations for hinge height $h = 12$ mm. a) Deformed geometry from FE simulation output. b) Stresses for $w = 10$ mm. c) Stresses for $w = 16$ mm.	22
21	a) Variation of maximum stresses at the apex with lateral hinge width for hinge height $h = 8$ mm. b) Apex strains showing type I fracture for $w = 6$ mm. c) Apex strains showing type I or type III fracture for $w = 8$ mm. d) Apex strains showing type III fracture for $w = 16$ mm.	23

22	Wider strain images for $h = 12$ mm and $w =$ a) 10 mm and b) 16 mm. Alternative fracture classification method.	23
23	Predicted type I to III transition bounds for two different fracture classification methods.	24
24	Post-operative model with labelled boundary conditions and constraints. Downwards load applied through centre of tibial plateau to mimic weight-bearing, and nodes in the vicinity of applied load point constrained to move as a rigid body.	25
25	Micromotion averaged over three locations at the cut entry with varying hinge width for three different hinge heights.	26
26	Fixation plate placements in MOWHTO. a) Anterior placement. b) Medial placement.	27
27	Proposed region for the osteotomy apex from the concatenation of (w, h) bounds, indicated by grey shading. Optimal location marked by X is at $w = 13$ mm, $h = 17$ mm, with a 2 mm radius circle to represent the accuracy of the saw cut. Hatching indicates areas which do not satisfy the proposed inequalities.	28
28	Both the proposed optimal apex region (blue outline) and the recommended region from literature (green region) mapped onto the surface of an average sized tibia. The osteotomy cut is shown in white, with its apex at the optimal point $w = 13$ mm, $h = 17$ mm.	29
29	Initial screw experiment setup with Perspex tibia. a) Labelled diagram of equipment setup. b) Image of setup taken during an experiment in the laboratory.	31
30	Revised experiment setup with metal tibia. a) Labelled diagram of equipment setup. b) Image of setup taken during an experiment in the laboratory.	32
31	Comparison between TomoFix fixation plate geometry and simplified plate geometry used in this investigation. All measurements in mm. a) TomoFix plate side view [21]. b) TomoFix plate front view with labelled holes [21]. c) Simplified plate geometry for default order. d) Simplified plate geometry for reverse order.	32
32	Vertical strains induced at the lateral hinge by the top, lag, and bottom screws, for insertion order ‘top, lag, bottom’. Four different screw tightening forces of 7, 10, 13, and 20 N were applied. Arrows indicate order of screwing.	33
33	Vertical strains induced at the middle of the lateral hinge by the top, lag, and bottom screws, for four different insertion orders. Two different screw tightening forces of 10 and 13 N were applied. Arrows and sub figure captions indicate order of screwing; screws in brackets indicate insertion without tightening. Order B negates tensile strains. Order C minimises overall strain magnitudes and is the optimal order.	34
34	Simplified model setup to investigate strains induced by the lag screw for screwing orders a) top, lag, bottom, and b) bottom, lag, top. Boundary conditions and constraints are labelled. Coupling constraints in red signify no translation or rotation between plate and tibia screw holes.	36
35	Simplified model setup to investigate strains induced by the top screw for screwing orders a) top, lag, bottom, and b) bottom, lag, top. Boundary conditions and constraints are labelled. Coupling constraints in red signify no translation or rotation between plate and tibia screw holes. Coupling constraints in green signify no translation between the plate and tibia screw holes, allowing rotation between them.	36

36	Mesh refinement at the lateral hinge and line (in white) along which strains were measured and plotted.	37
37	Strains predicted by FEA along the lateral hinge induced by the lag screw for the default and reverse screwing orders.	37
38	Strains predicted by FEA along the lateral hinge induced by the top screw for the default and reverse screwing orders.	38
39	Strains predicted by FEA along the lateral hinge induced by the lag screw for three different lag screw insertion angles relative to the horizontal axis. Default screwing order used in all cases.	40

List of Tables

1	Cortical and trabecular bone material properties used in simulations, based on [5]. E = Young's modulus, G = Shear modulus, and ν = Poisson's ratio.	19
2	Maximum von Mises stresses (GPa) for intra-operative simulations with different lateral hinge widths w , and heights h	46
3	Type I to type III transition points in (w, h) using the apex corner strain nucleation fracture classification method. Apex locations (w, h) which were not simulated are indicated by '-'.	46
4	Type I to type III transition points in (w, h) using the wider strain distribution fracture classification method.	46